



**HAL**  
open science

## Fluid pathways and high pressure metasomatism in a subducted continental slice (Mt. Emilius klippe, W. Alps)

Samuel Angiboust, Philippe Yamato, Solenn Hertgen, Thais Hyppolito, Gray E. Bebout, Luis F.G. Morales

### ► To cite this version:

Samuel Angiboust, Philippe Yamato, Solenn Hertgen, Thais Hyppolito, Gray E. Bebout, et al.. Fluid pathways and high pressure metasomatism in a subducted continental slice (Mt. Emilius klippe, W. Alps). *Journal of Metamorphic Geology*, 2017, 35 (5), pp.471-492. 10.1111/jmg.12241 . insu-01489148

**HAL Id: insu-01489148**

**<https://insu.hal.science/insu-01489148>**

Submitted on 6 Aug 2020

**HAL** is a multi-disciplinary open access archive for the deposit and dissemination of scientific research documents, whether they are published or not. The documents may come from teaching and research institutions in France or abroad, or from public or private research centers.

L'archive ouverte pluridisciplinaire **HAL**, est destinée au dépôt et à la diffusion de documents scientifiques de niveau recherche, publiés ou non, émanant des établissements d'enseignement et de recherche français ou étrangers, des laboratoires publics ou privés.

Received Date : 27-May-2016

Revised Date : 16-Nov-2016

Accepted Date : 27-Nov-2016

Article type : Original Article

## **Fluid pathways and high pressure metasomatism in a subducted continental slice (Mt. Emilius klippe, W. Alps)**

S. Angiboust<sup>1,5</sup>, P. Yamato<sup>2</sup>, S. Hertgen<sup>2</sup>, T. Hyppolito<sup>3</sup>, G. E. Bebout<sup>4</sup> and L. Morales<sup>1,6</sup>

<sup>1</sup> German Research Center for Geosciences (GFZ), Helmholtz Zentrum, Potsdam D-14473, Germany

<sup>2</sup> Géosciences Rennes, UMR 6118-CNRS, Université de Rennes 1, Rennes F-35042, France

<sup>3</sup> Universidade de São Paulo, Instituto de Geociências, Rua do Lago 562, Cidade Universitaria, 055508080, São Paulo, Brazil

<sup>4</sup> Department of Earth and Environmental Sciences, Lehigh University, Bethlehem, USA

<sup>5</sup> Institut de Physique du Globe de Paris, Sorbonne Paris Cité, Univ. Paris Diderot, CNRS, F-75005 Paris, France

<sup>6</sup> ETH, Auguste-Piccard-Hof 1, 8093 Zürich, Switzerland

*Journal of Metamorphic Geology*

This is the author manuscript accepted for publication and has undergone full peer review but has not been through the copyediting, typesetting, pagination and proofreading process, which may lead to differences between this version and the [Version of Record](#). Please cite this article as [doi: 10.1111/jmg.12241](https://doi.org/10.1111/jmg.12241)

This article is protected by copyright. All rights reserved

Short title: *Metasomatism in the eclogite-facies*

## **ABSTRACT**

The Mt. Emilius klippe (Western Alps, Italy) corresponds to a segment of the stretched Adriatic continental margin metamorphosed in granulite-facies during Permian. This slice was subducted during the early Cenozoic Alpine subduction with the underlying eclogite-facies remnants of the Tethyan seafloor (Zermatt-Saas zone). Near the base of the Mt. Emilius massif, there is a shear zone with eclogite-facies hydrofracture systems associated with deformation-induced re-equilibration of granulites during high pressure metamorphism. In the basal part of the massif, a pluri-hectometre domain of sheared mafic boudins is hosted in the granulitic paragneiss. In these mafic boudins there are garnetites, garnet veins and clinopyroxenite, as well as clinozoisite and calcite veins. These features record multiple events of fracture opening, brecciation, boudinage and parallelization of structures coevally with fluid-rock interaction, metasomatism and volume change. This integrated petrological, micro-textural and geochemical investigation illustrates the multiplicity and the chemical variability of fluid sources during prograde to peak metamorphic evolution in the lawsonite-

eclogite-facies field (at ~ 2.15-2.4 GPa, 500-550 °C) during subduction of the Mt. Emilius slice. The calcite veins crosscutting the garnetites have relatively low  $\delta^{18}\text{O}_{\text{VSMOW}}$  values (~ +6.5 ‰) near those for marble layers (and nearby calc-silicates) embedded within the metasomatized granulites (+8 to +10 ‰). It is proposed that infiltration of externally-derived H<sub>2</sub>O-rich fluids derived from the plate interface flushed the marbles, promoting decarbonation followed by short-distance transport and re-precipitation along garnetite fractures. This study highlights the importance of inherited structural heterogeneities (such as mafic bodies or sills) in localizing deformation, draining fluids from the downgoing plate, and creating long-lasting mechanical instabilities during subduction zone deformation.

Keywords: fluids, subduction, eclogite, Mt. Emilius, metasomatism

## INTRODUCTION

Fluids are known to play key roles in subduction interface processes, as demonstrated by field, experimental and geophysical observations (e.g. Prouteau *et al.*, 2001; John & Schenk, 2003; Audet & Burgmann, 2014). Metamorphic fluids produced by prograde dehydration of a downgoing slab have an impact on interplate coupling, seismicity distribution and arc magmatism (Schmidt & Poli, 1998; Peacock & Hyndman, 1999; Moreno *et al.*, 2014). Many studies have emphasized the close link between fluid release, fluid transport and the distribution of seismic events (Hacker *et al.*, 2003; Oncken *et al.*, 2003; Abers *et al.*, 2013). Jamtveit *et al.* (1990) demonstrated that pseudotachylytes (and seismicity) under eclogite-facies *P-T* conditions form through the re-equilibration of large volumes of subducted granulitic crust along shear zones in the presence of a fluid phase. The distribution of deformation, fluid flow and seismic activity within oceanic subduction zones under High Pressure (*HP*) conditions remains a matter of debate as well-preserved, large scale exposures documenting *HP* deformation are very rare (Philippot & Van Roermund, 1991; Stöckhert, 2002; Angiboust *et al.*, 2012; Deseta *et al.*, 2014). Both geophysical and field studies concur that fluids at near-lithostatic pore pressures (i) could maintain the subduction shear zone under low stress levels, and (ii) are highly channelized within shear zones and hydrofracture networks (e.g., Peacock *et al.*, 2011; Sibson, 2014; Angiboust *et al.*, 2015).

Fluid transport at *HP* conditions can lead to the formation of metasomatic reaction zones and selvages along fracture networks (Philippot & Selverstone, 1991; Hermann *et al.*, 2006; Zack & John, 2007). Natural examples of eclogite-facies fluid conduits are rare and their understanding is often limited by the relatively small dimensions of field exposures.

Detailed petrological and textural documentation of these unusual features are needed to highlight deep-seated tectonic processes and mass transfer across and along the subduction interface (e.g., Molina *et al.*, 2002; Ferrando *et al.*, 2009; Centrella *et al.*, 2015; Bebout & Penniston-Dorland, 2016).

In order to better document and understand mineralogical, fluid-rock interaction and fluid transport processes in deep subduction zone settings, we herein focus on an eclogite-facies shear zone within a slice of granulitized continental crust (Mt. Emilius klippe) in the Italian Western Alps. Previous work has shown that this shear zone provides a large-scale natural laboratory documenting deformation and fluid-rock interaction in the eclogite-facies (Pennacchioni, 1996; Scambelluri *et al.*, 1998) during subduction in the early Cenozoic. The aim of this work is to analyze the petrology of the structural development and mineralogy and bulk chemistry of the metasomatized rocks, so as to elucidate the composition and origin of the infiltrating fluid, relating these features to understand the evolution of fluid pathways during subduction.

## **GEOLOGICAL SETTING**

The internal zones of the W. Alps formed by the subduction of the Tethyan realm between c. 100 and 40 Ma (e.g. Coward & Dietrich, 1989; Dal Piaz *et al.*, 2001; Agard *et al.*, 2009). During this subduction process, thrust sheets of metasedimentary rocks and associated mafic/ultramafic lithologies were accreted in a subduction zone, forming the Liguro-Piemontese domain. The Zermatt-Saas unit (ZSU) constitutes the part of this nappe-stack that reached the highest pressure conditions at 50-45 Ma (2.3-2.6 GPa; Rubatto *et al.*, 1998; Lapen *et al.*, 2003; Bucher *et al.*, 2005; Angiboust *et al.*, 2009). Recent discoveries suggest that the hanging wall of the ZSU may represent a composite domain juxtaposing sub-km-scale tectonic slices with differing *P-T-t* histories (e.g., Lago di Cignana unit: Reinecke, 1991; Groppo *et al.*, 2009; Etirol-Levaz Unit (ELU): Fassmer *et al.*, 2016 and references therein). A few slices of continental affinity have been reported along this shear zone (ELU, Theodul Glacier Unit (TGU): Weber & Bucher, 2015; ChU, Chatillon Unit (ChU): Rolfo *et al.*, 2004; see also Ballèvre *et al.*, 1986; Fig. 1). Recent geochronological investigations revealed Alpine peak metamorphic ages (Lu-Hf: 60-50 Ma; Weber *et al.*, 2015; Fassmer *et al.*, 2016; Fig. 1) about 10 Ma older than the underlying ZSU. These remnants are generally viewed as extensional allochthons formed during the stretching of the continental margin of the Adriatic plate (e.g. Polino *et al.*, 1990; Dal Piaz *et al.*, 2001; Beltrando *et al.*, 2010) and later accreted along the Alpine subduction interface under eclogite-facies conditions. In these continental slices, remnants of Permian granulite-facies metamorphism (0.6-0.7 GPa; ~ 700 °C; Dal Piaz *et al.*, 1983) similar to those visible in the Ivrea Zone are preserved within the domains that

have not completely recrystallized during early Cenozoic Alpine *HP-LT* metamorphic overprint.

The Mt. Emilius klippe constitutes one of the largest continental outliers, now exposed in the southern part of the Aosta valley (Fig. 1a). This massif, which was underthrust by the ZSU, also contains granulite-facies paragneisses that were eclogitized during Alpine deformation (Compagnoni *et al.*, 1977; Dal Piaz *et al.*, 1983; Ballèvre *et al.*, 1986; Fig. 1b). Phengite Rb-Sr ages on Mt. Emilius micaschists yield ages of 50 to 40 Ma (Dal Piaz *et al.*, 2001). Based on the similarities in structures and tectono-metamorphic histories with the ELU, we hypothesize that the Mt. Emilius slice experienced peak-*P* metamorphism at c. 60-50 Ma. According to this, the shear zone at the base of the Mt. Emilius slice occupied a subduction interface hanging wall position during several Ma until the detachment from the downgoing slab and the underplating of the underlying *HP* ophiolites (ZSU). Extensive fluid-rock interaction features are therefore expected to occur along the hanging wall of the subduction interface (see also Angiboust *et al.*, 2014b).

The Mt. Emilius klippe is internally composed of a 2 km-thick sequence of felsic granulite-facies paragneiss with minor intercalations of mafic rocks and thin marble and calc-silicate layers (Bearth *et al.*, 1980; Pennacchioni, 1996; Fig. 1b). The main regional-scale schistosity, developed during prograde Alpine deformation at *HP* conditions, resulting in the pervasive recrystallization of pre-Alpine lithologies at the scale of the massif (>80 vol.%; Bearth *et al.*, 1980). This *HP* peak metamorphic event took place at 1.1-1.3 GPa and 450-550 °C according to Dal Piaz *et al.* (1983). During subduction, the host paragneisses (containing garnet, biotite, plagioclase and sillimanite; Dal Piaz *et al.*, 1983) were transformed to garnet-chloritoid micaschists. The original, granulite-facies paragenesis forming mafic lenses in the Mt. Emilius massif contains varying proportions of hornblende, diopside, plagioclase and garnet, and mafic boudins recrystallized into a garnet-omphacite-glaucophane-phengite assemblage during the *HP* alpine event (Pennacchioni, 1996; for a detailed petrographic description of Mt. Emilius mafic eclogites, see also Bearth *et al.*, 1980; Dal Piaz *et al.*, 1983). We focus here on the Arbole region (Fig. 1) where sheared remnants of an eclogitized mafic layer are exposed (Arbole Shear Zone: ASZ). This body is now strongly boudinaged, veined and wrapped by foliated micaschists (Pennacchioni, 1996). Two types of mafic eclogites are exposed in the Mt. Emilius massif (e.g. Scambelluri *et al.*, 1998). The one named “granulitized eclogites” by Pennacchioni (1996) preserves remnants of pre-alpine, granulite facies metamorphism now largely overprinted by the eclogite facies event. The second type of mafic eclogites is devoid of granulite-facies imprint and may represent sills or dyke systems that formed during the Early Mesozoic history (e.g. Mazzucchelli *et al.*, 2010). The spatial distribution and the relative amounts of the two different mafic lithotypes have not been documented yet. Scambelluri *et al.* (1998) showed that mafic eclogites richer

in total Na contain higher vein omphacite amounts, and concluded on the importance of locally-derived fluid flux during the veining process. These authors, who reported high salinity fluid inclusions (20-50 wt.% salts) trapped inside vein-filling clinopyroxene, proposed that various (mostly internal) fluid sources may have contributed to the mineralogical and geochemical signature of these mafic eclogites.

## ANALYTICAL METHODS

Electron probe microanalysis (EPMA) was performed using a JEOL-JXA 8230 probe at the GFZ Potsdam under standard analytical conditions (15 kV, 20 nA, wavelength-dispersive spectroscopy mode), using a 10 $\mu$ m beam. Standards used for the calibration were the following: orthoclase (Al, Si, K), fluorite (F), rutile (Ti), Cr<sub>2</sub>O<sub>3</sub> (Cr), wollastonite (Ca), albite (Na), MgO (Mg), Fe<sub>2</sub>O<sub>3</sub> (Fe) and rhodonite (Mn). X-ray mapping was undertaken at 15 kV and 30 nA, with a beam size of 2  $\mu$ m. Mineral abbreviations are given after Whitney & Evans (2010). Clinopyroxene naming follows the classification of Morimoto (1988). The following convention is used here for naming the numerous clinopyroxene generations in ASZ rocks: pre-alpine diopside: *Di*<sub>0</sub>, alpine diopside: *Di*, omphacite (only alpine): *Omp*, clinopyroxene: name given for all undifferentiated alpine clinopyroxenes. Pre-alpine garnet is named *Grt*<sub>0</sub> while the various generations of alpine garnet are named *Grt*<sub>1</sub> and *Grt*<sub>2</sub> based on textural arguments. The label “Grt” refers to an undifferentiated alpine garnet generation.

Sample imaging (back scattered electron mode) was performed using a Scanning Electron Microscope Ultra 55 Plus (Carl Zeiss) with 20 kV acceleration voltage and UltraDry SDD EDS detector. Sample surface composition estimates were obtained by averaging of four surface scan estimates (3 x 1.5 mm, 30 s counting time).

Nine bulk-rock chemical analyses were performed on samples from the Arbole sector. Major elements were analyzed at the GFZ Potsdam by X-ray fluorescence (XRF) on 1050 °C-dried samples, prepared as fused discs of Li tetraborate-metaborate (FLUXANA FX-X65, sample-to-flux ratio 1:6). A Panalytical Axios Advanced wavelength-dispersive spectrometer and matrix correction programs were used to calculate concentrations. H<sub>2</sub>O and CO<sub>2</sub> concentrations were calculated as loss on ignition.

For stable-isotope analyses, CO<sub>2</sub> gas from carbonate samples was prepared by dissolution in 100% phosphoric acid at 25 °C overnight, following McCrea (1950), and the cryogenically purified gas was analyzed in dual-inlet mode on a Finnigan MAT 252 mass spectrometer at Lehigh University. Oxygen and C isotope values are reported relative to Vienna standard mean ocean water (VSMOW) and PeeDee belemnite (VPDB), respectively. Proper standardization for these analyses was verified by analysis of various laboratory and international carbonate standards including NBS-19 (calcite;  $\delta^{18}\text{O}_{\text{VSMOW}} = +28.6\text{‰}$ ;  $\delta^{13}\text{C}_{\text{VPDB}}$

= +1.95‰). Uncertainties (expressed as  $1\sigma$ ) are  $\sim 0.15\text{‰}$  and  $\sim 0.10\text{‰}$  for  $\delta^{18}\text{O}$  and  $\delta^{13}\text{C}$ , respectively. For >150 analyses of one internal calcite standard (sample 8-3-7v, calcite vein) over a 10-year period, uncertainties (expressed as  $1\sigma$ ) were  $\sim 0.15\text{‰}$  and  $\sim 0.10\text{‰}$  for  $\delta^{18}\text{O}$  and  $\delta^{13}\text{C}$ , respectively.

## PETROLOGICAL OBSERVATIONS

### Field relationships in the Arbole region

The study area is located near the Rifugio Arbole, in the NW part of the Mt. Emilius massif (Fig. 1a). The host garnet micaschists (former felsic granulites) contain dismembered, decametre-scale ribbons of boudinaged mafic layers affected by mylonitic deformation during Alpine subduction (Pennacchioni, 1996). Locally, metre-sized boudinaged marble and calc-silicate layers are interleaved within the garnet micaschist sequence in the vicinity of the mafic boudins (Fig. 1b). We focus here on these sheared boudins, located  $\sim 100\text{m}$  structurally above the thrust contact separating the Mt. Emilius unit from the underlying Zermatt-Saas unit (Fig. 1). Mafic boudins are separated from the base of the Mt. Emilius klippe by a mylonitized domain comprising greenschists, retromorphosed eclogites and flattened quartz ribbons parallel to the main foliation (see also Dal Piaz *et al.*, 1983). The core of the Arbole Shear Zone (ASZ), less affected by retrogression, consists of a very heterogeneous mixture of centimetre- to metre-sized pods of garnetites, clinopyroxenites associated with clinozoisite-rich domains wrapped by an eclogite-facies foliation (Fig. 2a,b; see also Pennacchioni, 1996). The formation of mylonites, ultra-mylonites, crystal-preferred orientation in clinopyroxene and eclogite breccias (Fig. S1; Pennacchioni, 1996) point to pervasive shearing affecting the core of the ASZ.

### The vein systems in the Arbole region

All mafic lithologies in the Arbole region exhibit abundant fractures and vein systems filled by garnet, clinopyroxene or clinozoisite (Fig. 3). The mineralogy and the structural position of the various vein systems are shown in Table 1. Clinopyroxene veins, forming at high angle to the eclogitic foliation, are best preserved within domains sheltered from post-veining mylonitization. Many vein networks exhibit strong shearing that led to (i) their transposition parallel to the main foliation, (ii) the destruction of their original fibrous structure and (iii) the dynamic recrystallization of clinopyroxene and clinozoisite crystals leading to the development of a strong crystal-preferred orientation (CPO). When preserved from subsequent deformation, clinopyroxene, garnet and clinozoisite veins range in thickness from 2 mm to 5 cm (Fig. 3a). In the host granulite, fibrous clinopyroxene is associated with large blocky quartz crystals partly intergrown with *HP* minerals (Fig. 3b; Table 1). Calcite veins

containing euhedral grossular-rich garnet and automorphous clinopyroxene crystals cross-cut garnetite in the ASZ (Fig. 3c,d). Cross-cutting relationships between mafic eclogites and associated garnetite, omphacite and clinozoisite veins suggest several stages of vein opening and fracturing (Fig. 3e,f; Table 1). Clinozoisite-garnet-clinopyroxene domains (such as in Fig. 4a) exhibit numerous fracture networks filled by clinopyroxene and clinozoisite fibres. Locally, zones comprising angular clinopyroxenite clasts are enclosed within a clinozoisite-rich matrix (Fig. 4b,c). These field relationships suggest alternating brittle and ductile deformation that led to the reworking of veins networks, boudinage of garnetite clasts and their incorporation into an eclogite-facies foliation (Fig. 2).

### **Veining at the scale of the Mt. Emilius slice**

Extensive field investigations in the Mt. Emilius slice revealed the ubiquitous presence of cm-sized quartz, omphacite or garnet-bearing vein systems (localities BP, GR, SM, LA and also in GRU; see Fig. 1c; Table 1). Although Mt. Emilius rocks near the basal thrust are highly retrogressed and ductily deformed, vein abundance increases towards the lowermost 200 m of the Mt. Emilius slice, above the contact with the underlying ZSU. We focus and restrict the description to veins in which *HP* minerals have been found. These veins formed initially at high angle to the main Alpine foliation (e.g. Fig. 4d) and were progressively rotated into parallelism with the dominant foliation during prograde, peak and possibly retrograde metamorphism and deformation. High-*P* veins from Mt. Emilius felsic granulites are dominantly filled by elongate, blocky quartz crystals with locally omphacite needles perpendicular to the vein wall (Figs 3b & 4d,e). Rarely, cm-sized chloritoid crystals or mm- to cm-sized rutile needles are intergrown with quartz vein crystals (Fig. 4d). Field textures such as the ones shown in Fig. 4 suggest formation via hydrofracturing processes (e.g. Bons, 2001).

Unlike mafic rocks in the Arbole shear zone, the metre-sized mafic boudins disseminated within the Mt. Emilius paragneiss sequence (probably former mafic enclaves or dykes) exhibit only minor veining and, where veins are present, only one single vein generation perpendicular to the host rock foliation is present. The chemical nature of the host rock is correlated with the mineral species filling the veins: clinopyroxene and garnet veins mostly form in mafic layers while quartz-dominated veins are only observed in the felsic host rock (in line with Scambelluri *et al.* (1998) observations; Table 1).

### **Microscopic textures**

To investigate peak metamorphic replacement and metasomatic processes, 75 polished thin sections were examined from samples of the ASZ and the Mt. Emilius massif. GPS coordinates of samples are given in Table S1. Due to the variable fluid-rock interaction

imprint existing in ASZ mafic rocks that often led to complete disappearance of the granulite-facies remnants, it can be difficult to distinguish between eclogites and eclogitized granulites defined by Pennacchioni (1996). We therefore hereafter preferentially refer to ASZ eclogitized basic rocks as “mafic eclogites”.

Pre-alpine, granulite facies pseudomorphs after diopside  $Di_0$  are preserved in mafic eclogites shielded in garnetites (Fig. 5a,e). The pre-alpine  $Grt_0$ , frequently preserved in the host granulite, has not been found in the metasomatized mafic eclogites. Pre-alpine hornblende and plagioclase (see Dal Piaz *et al.*, 1983) have been completely replaced during the alpine stage. Our microstructural observations indicate coeval growth of garnet, clinozoisite, clinopyroxene, titanite and apatite during eclogite-facies deformation (Figs 5 & 6). Among the most striking features of ASZ rocks is the widespread formation of garnetite in and around mafic eclogites (Figs 1, 2 & S1). Garnetite clasts contain clinozoisite and clinopyroxene inclusions defining a weak to moderate foliation (Fig. 5a,b). Garnetite layers exhibit a very homogeneous texture devoid of euhedral crystals (Fig. 5c). A weakly-oriented “cement” that encapsulates oriented angular porphyroblasts of clinopyroxene and clinozoisite is composed of xenomorphic garnet grains of 5-10  $\mu\text{m}$  in diameter (Fig. 5c,d). In sample #14-15g, oriented titanite needles are parallel to the “intra-garnet foliation”. Clinopyroxene grew in textural equilibrium with garnet outer rims indicating that clinopyroxene crystals filled the porosity after garnet emplacement (see the white arrow in Fig. 5c). In most garnetite samples, pseudomorphs after pre-alpine diopside  $Di_0$  are visible in back-scattered electron images (Fig. 5e,f). Several generations of alpine diopside have been identified, progressively replacing the pre-alpine diopside crystals via micro-fracturing and pseudomorphic replacement along cleavage plans (Fig. 5f).

All minerals, including garnet, clinopyroxene, clinozoisite and titanite are zoned (Figs 5f & 6a,b). Where present, fractured titanite porphyroclasts are overgrown by another titanite generation together with apatite and clinozoisite (Fig. 6b). Micrometre-scale chemical oscillations are observed in most of ASZ minerals, seemingly representing incremental growth of minerals in equilibrium with a fluid phase. X-ray mapping shows numerous chemical oscillations of minor amplitude (Fig. 6c) for a garnet crystal growing along the wall of a calcite vein (Fig. 3d).

Vein-filling material exhibits variable textural patterns from static growth to extreme elongation (Figs 6d,e). Elongated clinopyroxene crystals (Fig. 6d) represent growth parallel to the clinopyroxene c-axis during vein opening (e.g., Pennacchioni, 1996; Bons *et al.*, 2012). Vein-filling garnet also traps stretched inclusions oriented perpendicular to the vein walls (Fig. 6f). Incremental, crack-seal features are also very common within clinopyroxene veins (Fig. 6e). Figure 6e exhibits static and incremental opening of the same vein network. The first opening event led to the precipitation of diopside (light grey) followed by omphacite (dark

grey; Fig. 6e). The second event disrupted the previous structure and healed the fragments by a clinopyroxene of intermediate composition. These two contrasting textural patterns reveal the recurrence of fracturing processes, associated with fluid circulation, operating within ASZ during eclogite-facies deformation.

Undeformed calcite veinlets, together with garnet, clinopyroxene, clinozoisite, titanite and apatite occur in garnetite samples (sample #15-06b; Fig. 3c,d). Calcite is also intergrown with diopside and grossular-rich garnet in calc-silicate layers at the contact with the host granulite. Rutile is present in mafic eclogites away from the ASZ, as well as a vein-filling mineral within quartz veins (Fig. 4d; Table 1). It is absent from the core of the ASZ, probably transformed to titanite during fluid-rock interaction. Numerous apatite crystals form ribbons parallel to the main foliation plane within ASZ mafic eclogites.

## MINERAL CHEMISTRY

### Garnet

Representative mineral compositions are given in Table 2. Garnet from former eclogitized granulites outside the ASZ preserves fractured and partially dissolved remnants of pre-Alpine metamorphism with the highest pyrope contents (~ 40 mol.% Prp; Fig. 7). The pre-Alpine garnet cores  $Grt_0$  show replacement by clinopyroxene, chlorite and quartz leading to the formation of an atoll structure (Fig. 7b). Note that the replacing Alpine garnet generation  $Grt_1$  lining the fractures has not been retrogressed (Fig. 7). This new  $Grt_1$  generation is richer than  $Grt_0$  in Ca, Fe and Mn (Fig. 7). Intra-garnet healed fractures show  $X_{Mg}$  decrease, but these fractures are not visible in the Ca X-ray map.

Prograde Alpine  $Grt_1$  from ASZ mafic eclogites is also found in some samples along the main foliation, exhibiting a core-to-rim decrease in Mn as well as omphacite inclusions (Fig. 8a,d). This prograde Alpine garnet ( $Grt_1$  in Fig. 8d) has been pervasively fractured, dissolved and replaced by a very fine-grained mixture of Grs-richer garnet ( $Grt_2$ ), clinopyroxene (mostly diopside) and clinozoisite (Fig. 8b). Garnet ( $Grt_1$ ) cores are sometimes completely dissolved leaving an atoll-like structure made of  $Grt_2$ . This latest ( $Grt_2$ ) is always much richer in Ca than  $Grt_1$  (from Grs60 to Grs80; Fig. 8c). Embayment and dissolution features are very frequent inside and around  $Grt_1$  remnants (Fig. 8d). Alpine mylonitic deformation sheared  $Grt_2$ -Cpx-Czo aggregates and disrupted the alpine, prograde  $Grt_1$  shape and angular garnet clasts have been disseminated along the main diopside-rich Alpine foliation (see Fig. 8c).

Garnet from garnetite layers exhibits a very complex zoning pattern, with only minor chemical variations. These garnetite domains show variable grossular contents between 45-50 mol.% and 70-90 mol.% (#14-12ha; #14-07, respectively; Table 2). Internal zoning structure comprises multiple garnet generations (Fig. 8e) as well as numerous stages of

growth and dissolution-precipitation. Vein-filling  $Grt_2$  (Fig. 3d) also shows a composition close to grossular end-member composition (70-75 mol.% Grs) with some almandine (12 mol.%), spessartine (2 mol.%) and andradite (12 mol.%) components. Low oxide analytical totals (98-99 wt.%) also suggest some minor hydrogrossular component.

### **Clinopyroxene**

Clinopyroxene from the mafic boudins outside the Arbole shear zone (ASZ) is omphacite and generally differs from most ASZ clinopyroxene by higher jadeite (Jd40-50 on average). More than ~90% of ASZ clinopyroxene crystals are diopside-rich (Di55-80) and jadeite-poor (Jd2-20; Fig. 9). This Di-rich clinopyroxene is found in all textural settings including (i) pseudomorphs after pre-Alpine diopside  $Di_0$  (Fig. 5a) (ii) included within garnetite layers and garnet veins (Figs 5c & 6f) (iii) included in Alpine garnet cores (iv) as vein-filling material and (v) along the main Alpine foliation. In ASZ mafic eclogites foliation, they show a complex zoning pattern with (i) overgrowth and replacement of omphacite cores and (ii) rimming by a slightly Na-richer composition (Jd14-18) near the rims. Diopside from the veins is sometimes closely associated with omphacite fibres (Figs 6d & 9). Some of the vein systems studied here exhibit in a single vein two to three chemically different clinopyroxene generations (Fig. 6d,e). A first diopside (Di60-65, Jd10-20) is overgrown by an omphacite-rich clinopyroxene (Di30-38, Jd42-50), which is later overgrown by a clinopyroxene of intermediate composition (Di42-48, Jd32-41). Omphacite is observed in all textural positions including metamorphic veins (Fig. 6d), pseudomorphs after pre-Alpine diopside  $Di_0$ , included within garnetite layers and Alpine garnet cores ( $Grt_1$ , Mn-rich domain on Fig. 8a,d) and as (rare) remnants along the main Alpine foliation. Even if it is clear that omphacite is more abundant in samples with higher bulk Na contents (in line with Scambelluri *et al.*, 1998), omphacite has been also observed in Na-depleted bulk rock compositions (e.g. Fig. 6e).

### **Other minerals**

In the ASZ mafic eclogites, clinozoisite exhibits relatively homogeneous compositions between Ps10-20. No systematic zoning trend in epidote has been observed among the samples. Several titanite generations have been noted with Al-poor cores (~ 1.5 wt.%) and Al-richer rims (2 - 3 wt.%  $Al_2O_3$ ; Fig. 6b). In foliated samples titanite contains between 2.5 and 3 wt.%  $Al_2O_3$  and Al-poor cores were not preserved. Calcite is nearly pure (~ 99% Ca) with minor amounts of Fe (0.05-0.1 wt.%) and Mn (0.03-0.06 wt.%). Phengite is extremely rare in ASZ mafic eclogites. A few, 10 $\mu$ m-large inclusions associated with omphacite (Jd45) and clinozoisite (Ps16) within  $Grt_1$  cores (sample #14-07a; Figs 8 & S1) exhibit high Si (~ 3.45 apfu; Table 2). Quartz is present as rare interstitial crystals in matrices of metasomatized ASZ samples and as inclusions within  $Grt_1$ . Zircon crystals are very rare and, where present, are smaller than 20 $\mu$ m.

## THERMOBAROMETRY

In order to re-evaluate peak metamorphic conditions of the Mt. Emilius massif as well as put  $P$ - $T$  constraints on the metasomatic event studied here, two key phengite-bearing mafic eclogites have been selected. The first sample (BP1504b) is a non-metasomatized, foliated mafic eclogite showing an alpine paragenesis of garnet, omphacite, phengite ( $Si = 3.44$ - $3.47$  apfu), glaucophane, clinozoisite and quartz, from the Bon Plan locality in the northeastern sector of Mt. Emilius klippe (BP on Fig. 1a). The second sample is a metasomatized mafic eclogite from the Arbole Shear Zone (#14-07; see Figs 8 & S1f for petrological information). The software THERMOCALC (v.3.33; average  $P$ - $T$  mode) using an updated version (2003) of the internally consistent database from Holland & Powell (1998) was used here (Powell & Holland, 1994). End member activities were calculated using the software AX running at  $550^\circ\text{C}$  and  $2.3$  GPa. The detailed, resulting dataset is presented in Table S2.

The average peak metamorphic  $P$ - $T$  for sample BP14-04b (non-metasomatized eclogite) is  $2.25 \pm 0.12$  GPa and  $533 \pm 15^\circ\text{C}$  ( $n =$  eight calculations) for the assemblage Omp-Phg- $Grt_1$ (rim)-Gln-Czo-Qz- $H_2O$ . Average peak metamorphic  $P$ - $T$  estimates for the sample #14-07 (metasomatized ASZ eclogite) have been calculated using  $Grt_1$  outer core composition, omphacite and phengite inclusions in  $Grt_1$  (Table 2; Figs 8 & S1), clinozoisite/lawsonite, quartz and  $H_2O$ . Given the uncertainty regarding the stability of lawsonite at peak conditions in this sample, we tried some calculations with and without the lawsonite end-member. The presence of lawsonite does not significantly change the  $P$ - $T$  estimates (slight temperature increase and pressure decrease; see Table S2). The obtained average conditions are  $546 \pm 23^\circ\text{C}$  /  $2.29 \pm 0.13$  GPa ( $n =$  seven calculations). The  $a(H_2O)$  has been reduced in steps to 0.9 to accommodate the report of saline inclusions in clinopyroxene (Scambelluri *et al.*, 1998) and due to the presence of minor amounts of calcite in these samples. Lowering  $a(H_2O)$  by 0.1 only yields  $5$ - $10^\circ\text{C}$  lower peak temperatures with almost no effect on pressure estimates. The decrease of water activity to 0.5 decreases temperature by  $20$ - $25^\circ\text{C}$ . Given the uncertainty on water activity at peak conditions in ASZ mafic eclogites (probably between 0.5 and 0.8; Scambelluri *et al.*, 1998; Warren & Waters, 2006), we conclude that the Mt. Emilius klippe reached peak  $P$ - $T$  of  $2.15$  -  $2.4$  GPa and  $500$  -  $550^\circ\text{C}$ , conditions overlapping with those for the underlying ZSU ( $540^\circ\text{C}$ ,  $2.3$  GPa; Angiboust *et al.*, 2009). These two  $P$ - $T$  estimates on Mt. Emilius klippe yield relatively similar results, showing that the metasomatic process affecting the ASZ occurred at or near the metamorphic peak pressure.

## GEOCHEMISTRY AND PHASE RELATIONSHIPS

A total of 28 bulk rock compositions of the Arbole region are presented in the CaO- $Na_2O$ -MgO diagram in Fig. 10 (bulk rock compositions are shown in Table 3). Data from

Scambelluri *et al.* (1998) for mafic eclogites from the ASZ region are shown, along with that from Ivrea mafic bodies from Sills & Tarney (1984) and Mazzucchelli *et al.* (1992). The chemical similarity between non-metasomatized Mt. Emilius mafic eclogites and Ivrea mafic bodies suggests that the latter represent the best equivalent to ASZ lithologies prior to Alpine subduction and fluid-rock interaction. This plot shows that (i) non-metasomatized eclogites from the Arbole region partially overlap the higher CaO compositions of the Ivrea mafic bodies (ii) metasomatism in the ASZ (green symbols) is characterized by a marked increase in Ca content and for most samples a decrease in Na and Mg (Fig. 10). Non-altered bulk rock compositions (from Scambelluri *et al.*, 1998, from Sills & Tarney, 1984 and from Mazzucchelli *et al.*, 1992) also reveal that K<sub>2</sub>O is removed during the metasomatic process (from 0.5 to 0.02 wt.% on average; see Table 3). Note that mass balance calculations could not be performed to quantitatively estimate element mobility in the ASZ because of (i) the uncertainty regarding the exact starting composition and (ii) the multiple stages of veining that affected the rock volume during alpine metamorphism. Phase relationships between minerals from ASZ metasomatized rocks and bulk rock compositions were considered in the ACF projection (Fig. 11). The ACF diagram has been designed using the Cspace software (Torres-Roldan *et al.*, 2000), projected from coexisting phases and appropriate vectors to represent the compositional space. Relevant end-members forming the solid solutions of interest have been plotted in order to compare with the chemistry of ASZ peak metamorphic minerals. This figure shows that most metasomatized bulk compositions can be decomposed in this projection by a mixture of garnet, clinopyroxene and epidote/clinozoisite. Phase relations for peak conditions are controlled by the degree of alteration of the rocks: for rocks richer in CaO and poorer in MgO (see also Fig. 10), there is a progressive shift of tie-lines from a less to more Ca-rich garnet, and from Al-rich clinopyroxene to diopside-rich compositions (i.e. from triangle A to triangle B on Fig. 11). Garnetite samples plot within and around the garnet solid solution line and clinopyroxenites plot along the tie-line connecting epidote and diopside. This projection shows that non-metasomatized compositions from Ivrea (black crosses on Fig. 11) and from the Arbole region (blue crosses) are often poorer in Ca than metasomatized ASZ rocks. Most non-metasomatized bulk compositions plot outside the triangle "A". A garnet with a more Grs-poor composition, an omphacite and a calcic amphibole are needed to satisfy equilibrium phase relations for these non-metasomatized compositions in this projection. Lastly, the shift of garnet compositions below the garnet tie line reflects the presence of some andradite molecule within the highest Grs content garnet (Fig. 11).

## **CARBON AND OXYGEN ISOTOPE COMPOSITIONS OF ASZ CARBONATES**

Carbon and O isotope compositions are important proxies that can elucidate fluid transfer

processes in metasomatic systems (e.g., Galvez *et al.*, 2013; Ague & Nicolescu, 2014; Collins *et al.*, 2015; Rubatto & Angiboust, 2015; Scambelluri *et al.*, 2016). The  $\delta^{13}\text{C}$  and  $\delta^{18}\text{O}$  values of three calcite-bearing *HP* veins were obtained in order to evaluate the isotopic compositions and potential source(s) of fluids infiltrating the ASZ (see Fig. 3d). The  $\delta^{13}\text{C}$  of the calcite veins ranges from -2.9 to -3.2‰ and  $\delta^{18}\text{O}$  ranges from +6.5 to +6.8‰ (Table S3). Four nearby samples of marble and calc-silicate layers embedded within the ASZ (Fig. 1c) have  $\delta^{18}\text{O}$  values of +7.8 to +9.6‰ respectively, slightly higher than the values for the veins (Table S3). Their  $\delta^{13}\text{C}$  values are also slightly higher than those of calcite veins, falling between -2.2 and -0.2‰. In Fig. 12, these C and O isotope compositions are compared with data for carbonate material from the Schistes Lustrés complex in the W. Alps (Zermatt-Saas and Monviso Units; ZSU and MV on Fig.12), which correspond to exhumed *HP* slices of metasedimentary, metabasaltic and ultramafic remnants of the Tethyan seafloor (e.g. Cook-Kollars *et al.*, 2014; Collins *et al.*, 2015). This material has been chosen for comparison because it represents a potential analogue to the subducting oceanic slab material constituting a major source of metamorphic fluids at *HP* conditions (e.g. Bebout & Penniston-Dorland, 2016). The O isotope compositions of the ASZ veins are nearer those of finely disseminated and fracture-filling calcite in ZSU mafic and ultramafic rocks, the latter with  $\delta^{18}\text{O}$  as low as +8‰, than to compositions of ZSU metasedimentary rock samples with  $\delta^{18}\text{O}$  >+15‰ (Fig.12).

## DISCUSSION

### High Pressure metasomatism and Ca mobility

Mafic eclogites from the Arbole region exhibit complex deformation associated to fluid-rock interactions that occurred under eclogite-facies conditions during Alpine subduction. A metasomatic event led to the nearly complete replacement of the pre-Alpine granulite-facies fabric by a very complex and heterogeneous mixture of garnet, clinopyroxene and clinozoisite (see also Putnis, 2009). This replacement led to a decrease in the number of minerals as theoretically expected for infiltration metasomatic processes (Korzhinskii, 1968). We postulate that the clinozoisite that pervasively formed in the Arbole shear zone (Figs 3f & 4b) as matrix and vein-filling material may have initially been lawsonite ( $\text{CaAl}_2\text{Si}_2\text{O}_7(\text{OH})_2 \cdot \text{H}_2\text{O}$ ) as suggested by the presence of lozenge-shaped pseudomorphs along a *HP* vein from the ASZ (Fig. S1; see also Dal Piaz *et al.*, 1983). Our peak metamorphic *P-T* estimates that fall within the lawsonite-eclogite-facies field support this conclusion and plot within the same *P-T* range as the underlying Zermatt-Saas unit (Groppo *et al.*, 2009; Angiboust & Agard, 2010). The crossing of the Lws-out reaction curve at 1.8 GPa during exhumation probably also released significant amounts of fluids (Fig. 1c). We hypothesize that the late amphibole-bearing fractures that ubiquitously cut at high angle

across the Mt. Emilius rocks *HP* foliation (Pennacchioni, 1996) may be the trace of this exhumation-related fluid escape.

This enrichment in lawsonite/clinozoisite under peak pressure conditions is important for understanding mass transfer in subduction zones and across the plate interface. All evidence suggests that ASZ mafic eclogites composition has been significantly changed during fluid-rock interaction, although some uncertainties remain regarding the exact pre-metasomatism composition. Phase relationships and comparison of non-metasomatized rocks from the Arbole region with mafic bodies compositions from the Ivrea zone shed light on their relationships (Figs 10 & 11). The most striking feature is the very high Ca content of ASZ rocks. Sills & Tarney (1984) noted that Ivrea amphibolites exhibit CaO mostly in the range 11 to 16 wt.% and attributed this to the composition of the parent basalt. Bulk-rock compositions for the ASZ mostly range between 17 and 28 wt.% CaO (Table 3), hence exceeding by up to 10-15 wt.% the CaO contents of the supposed protolith (see also the data from Mazzucchelli *et al.*, 1992). Bulk rock compositions also suggest that this Ca enrichment has been accompanied by the removal of MgO, Na<sub>2</sub>O and K<sub>2</sub>O from the pre-metasomatic system (Table 3). On the one hand, the relatively high Grs content of prograde Alpine cores (*Grt*<sub>1</sub>; ~50 mol.% Grs; Fig. 8c) confirms that the rock was already enriched in Ca before the metasomatic event. On the other hand, the presence of omphacite inclusions within the same *Grt*<sub>1</sub> cores (Figs 8d & 9) suggest that Na was not yet completely leached out from the rock at that stage. Calcium enrichment evidence from mineral zoning patterns (Figs 7 & 8) and bulk rock compositions (Figs 10 & 11) confirms that a fluid in disequilibrium with the host granulite has been added into the system during metamorphism at *HP/LT* conditions. We conclude that these mafic eclogites (that were already moderately pre-enriched in Ca before Alpine subduction) have undergone further Ca enrichment during prograde and peak Alpine metamorphism (i.e. within the jadeite stability field; Fig. 1c). Sodium and K leaching during *HP* fluid-rock interaction also explains the extreme scarcity of phengite and the decrease in clinopyroxene jadeite content with increasing metasomatic overprint (see also Scambelluri *et al.*, 1998).

This alteration pattern strikingly recalls previous field observations from the shear zone at base of the Dent Blanche nappe further north, interpreted as a fossil subduction interface that reached 1.1-1.3 GPa (Angiboust *et al.*, 2015). These authors reported strong Ca enrichment (and alkali removal) related to the infiltration of sedimentary-derived fluids and formation of clinozoisite veins within the shear zone at the base of this large orthogneissic slice. A similar alteration trend is reported in Alpine Corsica where a Permian orthogneissic body exhibits microstructural replacement features and geochemical imprints similar to ASZ rocks (Martin *et al.*, 2011). In their case, subduction-related fluid-rock interaction led to the formation of lawsonites (see also Vitale-Brovarone *et al.*, 2014). In the Alps, lawsonite veins

have been also reported in the Monviso massif associated with intra-slab fluid transport under eclogite-facies conditions (Angiboust *et al.*, 2011). Droop & Chavrit (2014) similarly correlated Ca-rich eclogite with some fluid-rock interaction processes in the Malenco massif (Northern Italy). Lastly, John *et al.* (2008) and Beinlich *et al.* (2010) documented an unusual example of a deep vein system in which metasomatic Ca enrichment led to the eclogitization of a blueschist in the Tian Shan massif. All these examples (i) confirm that deep fluid conduits may be tracked via metasomatic reactions in *HP* rocks (ii) support the concept that Ca is a mobile element in the fluid phase under *HP* conditions prone to precipitate as Ca-bearing phases within favorable sites such as veins or lithological interfaces.

### **Evidence for multiple fluid infiltration events**

The Arbole shear zone metasomatized eclogites exhibit a very broad variety of lithologies and numerous vein systems and garnetite layers. Field and microtextural observations suggest that these garnetite layers formed via the percolation of a fluid phase carrying the elemental compounds (such as Ca) necessary to precipitate Grs-rich garnet (Figs 5a-d & 6f). We stress that these garnetite layers formed during this Alpine metasomatic event along the ASZ as indicated (i) by the complex zoning pattern (Fig. 8e) that cannot survive due to intra-crystalline diffusion processes at temperatures estimated for the pre-Alpine metamorphism (~700 °C) (ii) by the absence of such Ca-rich garnetite pods in non-eclogitized Ivrea-like lithologies (e.g. Dal Piaz *et al.*, 1971, 1973). We also stress that the similarity between garnetite and vein-filling garnet compositions indicates that the vein-filling process took place simultaneously or shortly after garnetite formation (Fig. 8c). The precise composition of the fluid phase cannot be directly derived from the mineralogy of the vein-filling material (e.g. Spandler & Hermann, 2006). However, the existence of multiple and distinct fluid-rock interaction events in the ASZ can be inferred from (i) the complex elementary zoning (Fig. 8e), (ii) the absence of one unique metasomatic vector in the ACF projection (Fig. 11) as well as (iii) the multiplicity of vein compositions occurring along the ASZ (clinopyroxenites, garnetites, lawsonitites; Figs 6e & 12). In other words, it is likely that the fluid responsible for garnetite or lawsonitite formation was chemically distinct from that from which the fibrous, vein-filling clinopyroxene material precipitated.

Furthermore, the presence of calcite veins in equilibrium with the eclogite-facies matrix (Figs 3d & 6a) supports the idea that fluids of varying sources,  $X\text{CO}_2$  and  $X\text{H}_2\text{O}$  contents infiltrated these rocks during ASZ deformation. The O and C isotope compositions of marbles and calc-silicates from the ASZ are slightly higher than those for the ASZ calcite veins (see Fig 12). One possible scenario to explain this similarity is (i) the infiltration within the ASZ of  $\text{H}_2\text{O}$ -rich fluids produced by the dehydration of mafic and ultramafic lithologies from the underlying oceanic slab followed by (ii) the dissolution of carbonate from ASZ

marbles lenses and (iii) precipitation of the calcite-diopside-grossularite veins within garnetite fractures. Collins *et al.* (2015) suggested that the low  $\delta^{18}\text{O}$  values for some particularly highly-veined ZSU (and Monviso) metabasalts and ophicarbonates could reflect infiltration of the rocks by an  $\text{H}_2\text{O}$ -rich fluid with  $\delta^{18}\text{O}$  as low as +6.0‰ sourced in the slab mafic/ultramafic section. An  $\text{H}_2\text{O}$ -rich fluid equilibrated with a clinopyroxene/garnet source lithology (i.e., metabasaltic) at temperatures of 500-600°C would have  $\delta^{18}\text{O}$  about 0.5 to 1.5‰ higher than its source (based on the fractionation factors of Zheng, 1993, 1999), thus near +6.5 to +7.5‰ for a source rock with whole-rock values near +6‰. We suggest that fluids sourced in the slab section infiltrated the subduction interface underlying the gneissic Mt. Emilius massif, leading to large shifts in the  $\delta^{18}\text{O}$  of metasedimentary and other rocks along the interface. Such shifts have recently been identified at several other subduction interface localities in the Swiss and Italian Alps (see Jaeckel *et al.*, 2016). Some infiltration of these fluids into the base of the overlying Mt. Emilius massif could have led to the decarbonation of impure carbonates, and also dissolution of marble carbonate, and the generation of low- $\delta^{18}\text{O}$  calcite veins, with some combination of decarbonation and interaction with metasedimentary rocks leading to the low  $\delta^{13}\text{C}$  values of the veins, marbles, and calc-silicates investigated in this study.

Our suggested scenario for the redistribution of carbonate within the Mt. Emilius massif is similar to the *HP* carbonation process documented for metasomatic marbles in the Ligurian and Corsican Alps (Scambelluri *et al.*, 2016; Piccoli *et al.*, 2016). At these localities, the C fraction of the metamorphic fluid, released by decarbonation and possibly also carbonate dissolution, was trapped within favourable sites during percolation through heterogeneous lithologies at depth. Finally, the absence of aegyrine enrichment in clinopyroxene and the absence of pistacite enrichment in epidote crystal rims suggest (i) that these fluctuating fluid compositions reported here were relatively reducing and (ii) that the O fugacity of the fluid phase has not significantly changed during the course of the metasomatic process in the ASZ.

### **Coupled metasomatic-deformation processes**

Field relationships demonstrate that the mafic bodies in the Arbole region played a singular role on fluid transport modalities, channeling fluids within the ASZ during *HP* deformation. It is likely that deformation and fluids were localized therein due to the presence of a viscosity contrast between the eclogitizing Arbole mafic body, which is stronger in comparison to the host garnet micaschists. Shearing and flattening associated with Alpine mylonitic deformation led to boudinage, disruption of the mafic layer and collection of metamorphic fluids (probably in the boudin neck regions). Later shearing reworked these primary structures that have been completely transposed in the actual ASZ rock record. We hypothesize that pervasive

fluid influx helped by local fracturing within the proto-Arbole shear zone triggered the formation of garnetites within outer mafic boudins (Fig. S1). Garnetite formation from a metamorphosed mafic protolith leads to an important volume reduction. Density calculations using the spreadsheet of Hacker & Abers (2004) for a partly eclogitized mafic boudin ( $\rho = 3.15 \text{ g cm}^{-3}$ ) and a Ca-rich garnetite layer ( $\rho = 3.6 \text{ g cm}^{-3}$ ) results in a ~15 % volume reduction. This mechanism could be responsible for the “collapse breccia” structure, draining surrounding metamorphic fluids within this newly-formed porosity. This fluid draining increased fluid-rock interaction and ultimately led to more garnetite formation and further porosity creation. Such “self-accelerating” density increase mechanism may explain the channeling along the ASZ of the very large amounts of fluids needed to generate the observed metasomatism (also see Yardley, 2009). The report of breccia-like structures (Fig. S1) suggests that this progressive replacement process was accompanied by shearing and clast rotation. Once the coherent pre-Alpine mafic layer was disrupted, this metasomatized shear zone has been continuously re-used during ductile Alpine deformation as shown by pervasive mylonitic and ultra-mylonitic networks (Fig. 2c; see also Pennacchioni, 1996).

#### **Fluid and deformation pathways in the eclogite field**

Scambelluri *et al.* (1998) proposed, based on the finding of Cl-bearing fluid inclusions in ASZ veins, that a pre-subduction hydrothermal stage may have (partially) re-hydrated the granulite. Such a hydration event would likely localize along fault zones during the rifting stage (e.g. Canales *et al.*, 2007) and trigger the complete chloritization of granulite-facies garnet crystals. Although dehydration of metamorphic pre-alpine products may have contributed to the total water budget, it is clear that the amount of H<sub>2</sub>O-rich fluids needed to transform the bulk of Mt. Emilius granulites into garnet micaschists is so large that the involvement of external fluids during the subduction stage is required to enable such a massive hydration event.

The strong rheology contrast between ASZ eclogites and the host micaschists is believed to have triggered the fracturing pattern reported here (veins, breccias), and therefore permitted an extreme fluid flow channelization along the Arbole Shear Zone under *HP* conditions (Fig. 13). Interface-parallel shear zone collection of slab-derived metamorphic fluids has been already reported in other places, such as in the Syros mélangé (Breeding *et al.*, 2004), in the Monviso Lower Shear zone (Angiboust *et al.*, 2014a) and in the Sesia zone (Konrad-Schmolke *et al.*, 2011), for instance. Despite a pervasive, exhumation-related regional metamorphic overprint along the shear zone at the base of the Mt. Emilius massif, the network of *HP* hydro-fractures cutting through pre-alpine (Fig. 3b) and alpine (Fig. 4d) fabrics is important for reconstructing the trajectory followed by fluids in subduction interfaces (Fig. 13). We hypothesize that these veins represent former fractures that enabled the fluid

phase to be transported from the dehydrating downgoing slab towards the core of the coherent Mt. Emilius tectonic slice (see also Davies, 1999). Our results also suggest that lateral heterogeneities such as the ASZ mafic layer may constitute under certain conditions a favorable locus for stress localization, fluid infiltration and formation of brittle features in a ductile environment (e.g. Mancktelow & Pennacchioni, 2005; Pennacchioni & Mancktelow, 2007).

The process of eclogitization of a granulite massif recalls the well-known Holsnøy Island occurrence within the Bergen Arcs (Caledonides, Norway) where eclogite-facies pseudotachylytes have been reported (Austrheim, 1987). The absence of frictional melting and pseudotachylytes in the Mt. Emilius massif may be related to the smaller size of the subducted continental unit and to the greater availability of fluids in the subduction environment. We conclude that tectonic brecciation associated with fluid circulation could represent a more likely mechanism to accommodate fast slip along shear zones in the eclogite field.

## **CONCLUSIONS**

The Mt. Emilius massif constitutes a remarkable, well-exposed natural laboratory to visualize progressive replacement and hydration of a granulitic crust in an oceanic subduction zone setting and to understand eclogite-facies deformation patterns. Mafic boudins embedded within garnet micaschists were metasomatized during the subduction of a slice of granulite-facies continental crust. Extensive fluid-rock interaction is evidenced by the formation of Ca-rich parageneses at the expense of pre-Alpine mafic assemblages, and multiple veining events in the lawsonite-eclogite-facies (500-550 °C, 2.15-2.4 GPa). Microstructural, petrological and geochemical data indicate the presence of varied fluid sources throughout the tectonic evolution of the Arbole Shear Zone, most likely derived from the underlying *HP* ophiolites from the Zermatt-Saas unit. This example highlights the nature and the structure of *HP* fluids pathways in the plate interface region of subduction zones and demonstrates how deep shear zones are used to transfer metamorphic fluids into the roots of the overriding plate.

## **ACKNOWLEDGMENTS**

This project has been funded by a GFZ internal grant to S.A. and by a INSU SYSTER grant to P.Y. M. Burn, M. Scambelluri and M. Ballèvre are thanked for insightful discussions. T.H. acknowledges FAPESP for a post-doctoral scholarship (2014/23422-0). Isotope analyses conducted at Lehigh University were supported by National Science Foundation grant EAR-1119264 (to GEB). Two anonymous reviewers as well as the journal editor D. Robinson are

acknowledged for their constructive comments on this manuscript. This is IPGP contribution #38XX.

## REFERENCES

- Abers, G. A., Nakajima, J., van Keken, P. E., Kita, S. & Hacker, B. R., 2013. Thermal–petrological controls on the location of earthquakes within subducting plates. *Earth and Planetary Science Letters*, **369**, 178-187.
- Agard, P., Yamato, P., Jolivet, L. & Burov, E., 2009. Exhumation of oceanic blueschists and eclogites in subduction zones: timing and mechanisms. *Earth-Science Reviews*, **92**, 53-79.
- Ague, J. J. & Nicolescu, S., 2014. Carbon dioxide released from subduction zones by fluid-mediated reactions. *Nature Geoscience*, **7**, 355-360.
- Angiboust, S. & Agard, P., 2010. Initial water budget: The key to detaching large volumes of eclogitized oceanic crust along the subduction channel? *Lithos*, **120**, 453-474.
- Angiboust, S., Agard, P., Yamato, P. & Raimbourg, H., 2012. Eclogite breccias in a subducted ophiolite: A record of intermediate-depth earthquakes? *Geology*, **40**, 707-710.
- Angiboust, S., Kirsch, J., Oncken, O., Glodny, J., Monié, P. & Rybacki, E., 2015. Probing the transition between seismically coupled and decoupled segments along an ancient subduction interface. *Geochemistry, Geophysics, Geosystems*, **16**, 1905-1922.
- Angiboust, S., Pettke, T., De Hoog, J. C., Caron, B. & Oncken, O., 2014a. Channelized fluid flow and eclogite-facies metasomatism along the subduction shear zone. *Journal of Petrology*, **55**, 883-916.
- Angiboust, S., Glodny, J., Oncken, O. & Chopin, C., 2014b. In search of transient subduction interfaces in the Dent Blanche–Sesia Tectonic System (W. Alps). *Lithos*, **205**, 298-321.
- Angiboust, S., Agard, P., Jolivet, L. & Beyssac, O., 2009. The Zermatt-Saas ophiolite: the largest (60-km wide) and deepest (c. 70–80 km) continuous slice of oceanic lithosphere detached from a subduction zone? *Terra Nova*, **21**, 171-180.
- Angiboust, S., Agard, P., Raimbourg, H., Yamato, P. & Huet, B., 2011. Subduction interface processes recorded by eclogite-facies shear zones (Monviso, W. Alps). *Lithos*, **127**, 222-238.
- Audet, P. & Bürgmann, R. 2014. Possible control of subduction zone slow-earthquake periodicity by silica enrichment. *Nature*, **510**, 389-392.
- Austrheim, H., 1987. Eclogitization of lower crustal granulites by fluid migration through shear zones. *Earth and Planetary Science Letters*, **81**, 221-232.

- Ballèvre, M., Kienast, J. R. & Vuichard, J. P. 1986. La «nappe de la Dent-Blanche» (Alpes occidentales): deux unités austroalpines indépendantes. *Eclogae Geologicae Helvetiae*, **79**, 57-74.
- Bearth, P., Dal Piaz, G. V., Elter, G., Gosso, G. & Martinotti, G., 1980. Il lembo di ricoprimento del Monte Emilius. Dent Blanche. *Atti della Reale Accademia delle scienze di Torino*, **114**, 226-240.
- Bebout, G. E., & Penniston-Dorland, S. C. 2016. Fluid and mass transfer at subduction interfaces—The field metamorphic record. *Lithos*, **240**, 228-258.
- Beinlich, A., Klemd, R., John, T. & Gao, J., 2010. Trace-element mobilization during Ca-metasomatism along a major fluid conduit: eclogitization of blueschist as a consequence of fluid–rock interaction. *Geochimica et Cosmochimica Acta*, **74**, 1892-1922.
- Beltrando, M., Rubatto, D. & Manatschal, G., 2010. From passive margins to orogens: The link between ocean-continent transition zones and (ultra) high-pressure metamorphism. *Geology*, **38**, 559-562.
- Bons, P. D., 2001. The formation of large quartz veins by rapid ascent of fluids in mobile hydrofractures. *Tectonophysics*, **336**, 1-17.
- Bons, P. D., Elburg, M. A. & Gomez-Rivas, E., 2012. A review of the formation of tectonic veins and their microstructures. *Journal of Structural Geology*, **43**, 33-62.
- Breeding, C. M., Ague, J. J. & Bröcker, M., 2004. Fluid–metasedimentary rock interactions in subduction-zone mélange: implications for the chemical composition of arc magmas. *Geology*, **32**, 1041-1044.
- Brovarone, A. V., Alard, O., Beyssac, O., Martin, L. & Picatto, M., 2014. Lawsonite metasomatism and trace element recycling in subduction zones. *Journal of Metamorphic Geology*, **32**, 489-514.
- Bucher, K., Fazis, Y., Capitani, C. D. & Grapes, R., 2005. Blueschists, eclogites, and decompression assemblages of the Zermatt-Saas ophiolite: High-pressure metamorphism of subducted Tethys lithosphere. *American Mineralogist*, **90**, 821-835.
- Canales, J.P., Sohn, R.A. & Demartin, B.J., 2007. Crustal structure of the Trans-Atlantic Geotraverse (TAG) segment (Mid-Atlantic Ridge, 26° 10' N): Implications for the nature of hydrothermal circulation and detachment faulting at slow spreading ridges. *Geochemistry, Geophysics, Geosystems*, **8**, 10.1029/2007GC001629.
- Cartwright, I. & Barnicoat, A. C., 1999. Stable isotope geochemistry of Alpine ophiolites: a window to ocean-floor hydrothermal alteration and constraints on fluid–rock interaction during high-pressure metamorphism. *International Journal of Earth Sciences*, **88**, 219–235.
- Centrella, S., Austrheim, H. & Putnis, A., 2015. Coupled mass transfer through a fluid phase and volume preservation during the hydration of granulite: An example from the Bergen

Arcs, Norway. *Lithos*, **236**, 245-255.

- Collins, N. C., Bebout, G. E., Angiboust, S. *et al.*, 2015. Subduction zone metamorphic pathway for deep carbon cycling II: Evidence from HP/UP metabasaltic rocks and ophiocarbonates. *Chemical Geology*, **412**, 132-150.
- Compagnoni, R., 1977. The Sesia-Lanzo Zone: high pressure–low temperature metamorphism in the Austroalpine continental margin. *Rendiconti della Societa Italiana di Mineralogia e Petrologia* **33**, 335–374.
- Cook-Kollars, J., Bebout, G. E., Collins, N. C., Angiboust, S. & Agard, P., 2014. Subduction zone metamorphic pathway for deep carbon cycling I: Evidence from HP/UHP metasedimentary rocks, Italian Alps. *Chemical Geology*, **386**, 31-48.
- Coward, M. & Dietrich, D., 1989. Alpine tectonics—an overview. *Geological Society, London, Special Publications*, **45**, 1-29.
- Dal Piaz, G., Cortiana, G., Del Moro, A., Martin, S., Pennacchioni, G. & Tartarotti, P., 2001. Tertiary age and paleostructural inferences of the eclogitic imprint in the Austroalpine outliers and Zermatt–Saas ophiolite, western Alps. *International Journal of Earth Sciences*, **90**, 668-684.
- Dal Piaz, G. V., Gosso, G. & Lombardo, B., 1983. Metamorphic evolution of the Mt. Emilius klippe, Dent Blanche nappe, western Alps, *American Journal of Science*, **283A**, p.438-458
- Dal Piaz, G.V., Gosso, G. & Martinotti, G., 1971. La II zona diorito-kinzigitica tra la valsesia e la Valle d'ayas (Alpi Occidentali). *Societa Geologica Italiana Memorie*, **10**, 257-276.
- Davies, J. H. 1999. The role of hydraulic fractures and intermediate-depth earthquakes in generating subduction-zone magmatism. *Nature*, **398**, 142-145.
- Deseta, N., Ashwal, L. D. & Andersen, T. B., 2014. Initiating intermediate-depth earthquakes: Insights from a HP–LT ophiolite from Corsic. *Lithos*, **206**, 127-146.
- Droop, G. T. & Chavrit, D., 2014. Eclogitic metagabbro from the Lanzada Window, eastern Central Alps: confirmation of subduction beneath the Malenco Unit. *Swiss Journal of Geosciences*, **107**, 113-128.
- Fassmer, K., Obermüller, G., Nagel, T. J. *et al.*, 2016. High-pressure metamorphic age and significance of eclogite-facies continental fragments associated with oceanic lithosphere in the Western Alps (Etirol-Levaz Slice, Valtournenche, Italy). *Lithos*, **252**, 145-159.
- Ferrando, S., Frezzotti, M. L., Petrelli, M., & Compagnoni, R. 2009. Metasomatism of continental crust during subduction: the UHP whiteschists from the Southern Dora-Maira Massif (Italian Western Alps). *Journal of Metamorphic Geology*, **27**, 739-756.
- Galvez, M. E., Martinez, I., Beyssac, O., Benzerara, K., Agrinier, P. & Assayag, N., 2013. Metasomatism and graphite formation at a lithological interface in Malaspina (Alpine

- Corsica, France). *Contributions to Mineralogy and Petrology*, **166**, 1687-1708.
- Gao, J., John, T., Klemd, R. & Xiong, X., 2007. Mobilization of Ti–Nb–Ta during subduction: evidence from rutile-bearing dehydration segregations and veins hosted in eclogite, Tianshan, NW China. *Geochimica et Cosmochimica Acta*, **71**, 4974-4996.
- Groppo, C., Beltrando, M. & Compagnoni, R., 2009. The *P–T* path of the ultra-high pressure Lago di Cignana and adjoining high-pressure meta-ophiolitic units: insights into the evolution of the subducting Tethyan slab. *Journal of Metamorphic Geology*, **27**, 207-231.
- Hacker, B. R., Abers, G. A. & Peacock, S. M., 2003. Subduction factory 1. Theoretical mineralogy, densities, seismic wave speeds, and H<sub>2</sub>O contents. *Journal of Geophysical Research: Solid Earth*, **108**(B1).
- Hacker, B. R. & Abers, G. A., 2004. Subduction Factory 3: An Excel worksheet and macro for calculating the densities, seismic wave speeds, and H<sub>2</sub>O contents of minerals and rocks at pressure and temperature. *Geochemistry, Geophysics, Geosystems*, **5**.
- Hermann, J., Spandler, C., Hack, A. & Korsakov, A. V., 2006. Aqueous fluids and hydrous melts in high-pressure and ultra-high pressure rocks: implications for element transfer in subduction zones. *Lithos*, **92**, 399-417.
- Holland, T. J. B. & Powell, R., 1998. An internally consistent thermodynamic data set for phases of petrological interest. *Journal of metamorphic Geology*, **16**, 309-343.
- Jaeckel, K. P., Bebout, G. E. & Angiboust, S., 2016. Carbon mobility at subduction interfaces via deformation-enhanced fluid infiltration: Evidence from the Swiss/Italian Alps, *American Geophysical Union Fall Meeting, San Francisco*, abstract **T31E-2946**.
- Jamtveit, B., Bucher-Nurminen, K. & Austrheim, H., 1990. Fluid controlled eclogitization of granulites in deep crustal shear zones, Bergen arcs, Western Norway. *Contributions to Mineralogy and Petrology*, **104**, 184-193.
- John, T. & Schenk, V., 2003. Partial eclogitisation of gabbroic rocks in a late Precambrian subduction zone (Zambia): prograde metamorphism triggered by fluid infiltration. *Contributions to Mineralogy and Petrology*, **146**, 174-191.
- John, T., Klemd, R., Gao, J. & Garbe-Schönberg, C. D., 2008. Trace-element mobilization in slabs due to non steady-state fluid–rock interaction: constraints from an eclogite-facies transport vein in blueschist (Tianshan, China). *Lithos*, **103**, 1-24.
- Klemd, R., 2013. Metasomatism during high-pressure metamorphism: eclogites and blueschist-facies rocks. In *Metasomatism and the Chemical Transformation of Rock* (pp. 351-413). Springer Berlin Heidelberg.
- Konrad-Schmolke, M., O'Brian P.J. & Zack, T., 2011. Fluid migration above a subducted slab – constraints on amount, pathways and major element mobility from partially overprinted eclogite-facies rocks (Sesia zone, Western Alps). *Journal of Petrology*, **52**, 455-486.
- Korzinskii, D. S., 1968. The theory of metasomatic zoning. *Mineralium deposita*, **3**, 222-231.

- Lapen, T. J., Johnson, C. M., Baumgartner, L. P., Mahlen, N. J., Beard, B. L. & Amato, J. M., 2003. Burial rates during prograde metamorphism of an ultra-high-pressure terrane: an example from Lago di Cignana, western Alps, Italy. *Earth and Planetary Science Letters*, **215**, 57-72.
- McCrea, J.M., 1950, The isotopic chemistry of carbonates and paleotemperatures scale. *Journal of Chemical Physics*, **18**, 849-857.
- Mancktelow, N.S. & Pennacchioni, G., 2005. The control of precursor brittle fracture and fluid-rock interaction on the development of single and paired ductile shear zones. *Journal of Structural Geology*, **27**, 645– 661.
- Martin, L. A., Rubatto, D., Brovarone, A. V. & Hermann, J., 2011. Late Eocene lawsonite-eclogite facies metasomatism of a granulite sliver associated to ophiolites in Alpine Corsic. *Lithos*, **125**, 620-640.
- Mazzucchelli, M., Rivalenti, G., Vannucci, R. *et al.*, 1992. Trace element distribution between clinopyroxene and garnet in gabbroic rocks of the deep crust: An ion microprobe study. *Geochimica et Cosmochimica Acta*, **56**, 2371-2385.
- Mazzucchelli, M., Zanetti, A., Rivalenti, G., Vannucci, R., Correia, C. T. & Tassinari, C. C. G., 2010. Age and geochemistry of mantle peridotites and diorite dykes from the Baldissero body: Insights into the Paleozoic–Mesozoic evolution of the Southern Alps. *Lithos*, **119**, 485-500.
- Morimoto, N., 1988. Nomenclature of pyroxenes. *Mineralogy and Petrology*, **39**, 55-76.
- Molina, J. F., Austrheim, H., Glodny, J. & Rusin, A., 2002. The eclogites of the Marun–Keu complex, Polar Urals (Russia): fluid control on reaction kinetics and metasomatism during high P metamorphism. *Lithos*, **61**, 55-78.
- Moreno, M., Haberland, C., Oncken, O., Rietbrock, A., Angiboust, S. & Heidbach, O., 2014. Locking of the Chile subduction zone controlled by fluid pressure before the 2010 earthquake. *Nature Geoscience*, **7**, 292-296.
- Oncken, O., Asch, G., Haberland, C. *et al.*, Seismic imaging of a convergent continental margin and plateau in the central Andes (Andean Continental Research Project 1996 (ANCORP'96)). *Journal of Geophysical Research: Solid Earth*, **108**(B7).
- Peacock, S. M. & Hyndman, R. D., 1999. Hydrous minerals in the mantle wedge and the maximum depth of subduction thrust earthquakes. *Geophysical Research Letters*, **26**, 2517-2520.
- Peacock, S. M., Christensen, N. I., Bostock, M. G. & Audet, P., 2011. High pore pressures and porosity at 35 km depth in the Cascadia subduction zone. *Geology*, **39**, 471-474.
- Pennacchioni, G., 1996. Progressive eclogitization under fluid-present conditions of pre-Alpine mafic granulites in the Austroalpine Mt Emilius Klippe (Italian Western Alps).

- Journal of Structural Geology*, **18**, 549-561.
- Pennacchioni, G. & Mancktelow, N.S., 2007. Nucleation and initial growth of a shear zone network within compositionally and structurally heterogeneous granitoids under amphibolite facies conditions. *Journal of Structural Geology*, **29**, 1757–1780, doi:10.1016/j.jsg.2007.06.002.
- Philippot, P. & Selverstone, J., 1991. Trace-element-rich brines in eclogitic veins: implications for fluid composition and transport during subduction. *Contributions to Mineralogy and Petrology*, **106**, 417-430.
- Philippot, P. & van Roermund, H. L., 1992. Deformation processes in eclogitic rocks: evidence for the rheological delamination of the oceanic crust in deeper levels of subduction zones. *Journal of structural geology*, **14**, 1059-1077.
- Piccoli, F., Brovarone, A. V., Beyssac, O., Martinez, I., Ague, J.J. & Chaduteau, C., 2016. Carbonation by fluid–rock interactions at high-pressure conditions: Implications for carbon cycling in subduction zones. *Earth and Planetary Science Letters*, **445**, 146-159.
- Polino, R., Dal Piaz, G. V. & Gosso, G., 1990. Tectonic erosion at the Adria margin and accretionary processes for the Cretaceous orogeny of the Alps. *Mémoires de la Société géologique de France*, **156**, 345-367.
- Powell, R. & Holland, T., 1994. Optimal geothermometry and geobarometry. *American Mineralogist*, **79**, 120-133.
- Prouteau, G., Scaillet, B., Pichavant, M. & Maury, R., 2001. Evidence for mantle metasomatism by hydrous silicic melts derived from subducted oceanic crust. *Nature*, **410**, 197-200.
- Putnis, A., 2009. Mineral replacement reactions. *Reviews in Mineralogy and Geochemistry*, **70**, 87-124.
- Reinecke, T., 1991. Very-high-pressure metamorphism and uplift of coesite-bearing metasediments from the Zermatt-Saas zone, Western Alps. *European Journal of Mineralogy*, **7**, 7-18.
- Rolfo, F., Compagnoni, R. & Tosoni, D., 2004. Geology and petrology of the Austroalpine Châtillon slice, Aosta valley, western Alps. *Geodinamica Acta*, **17**, 91-105.
- Rubatto, D., Gebauer, D. & Fanning, M., 1998. Jurassic formation and Eocene subduction of the Zermatt–Saas-Fee ophiolites: implications for the geodynamic evolution of the Central and Western Alps. *Contributions to Mineralogy and Petrology*, **132**, 269-287.
- Rubatto, D. & Angiboust, S., 2015. Oxygen isotope record of oceanic and high-pressure metasomatism: a P–T–time–fluid path for the Monviso eclogites (Italy). *Contributions to Mineralogy and Petrology*, **170**, 1-16.
- Scambelluri, M., Bebout, G. E., Belmonte, D. *et al.*, 2016. Carbonation of subduction-zone serpentinite (high-pressure ophicarbonates; Ligurian Western Alps) and implications for the

- deep carbon cycling. *Earth and Planetary Science Letters*, **441**, 155-166.
- Scambelluri, M., Pennacchioni, G. & Philippot, P., 1998. Salt-rich aqueous fluids formed during eclogitization of metabasites in the Alpine continental crust (Austroalpine Mt. Emilius unit, Italian western Alps). *Lithos*, **43**, 151-167.
- Schmidt, M. W. & Poli, S., 1998. Experimentally based water budgets for dehydrating slabs and consequences for arc magma generation. *Earth and Planetary Science Letters*, **163**, 361-379.
- Sibson, R. H., 2014. Earthquake rupturing in fluid-overpressured crust: How common? *Pure and Applied Geophysics*, **171**, 2867-2885.
- Sills, J. D. & Tarney, J., 1984. Petrogenesis and tectonic significance of amphibolites interlayered with metasedimentary gneisses in the Ivrea Zone, Southern Alps, Northwest Italy. *Tectonophysics*, **107**, 187-206.
- Spandler, C. & Hermann, J., 2006. High-pressure veins in eclogite from New Caledonia and their significance for fluid migration in subduction zones. *Lithos*, **89**, 135-153.
- Stöckhert, B., 2002. Stress and deformation in subduction zones: insight from the record of exhumed metamorphic rocks. *Geological Society, London, Special Publications*, **200**, 255-274.
- Torres-Roldan, R. L., Garcia-Casco, A. & Garcia-Sanchez, P. A., 2000. CSpace: an integrated workplace for the graphical and algebraic analysis of phase assemblages on 32-bit Wintel platforms. *Computers & Geosciences*, **26**, 779-793.
- Warren, C. J. & Waters, D. J., 2006. Oxidized eclogites and garnet-blueschists from Oman: P-T path modelling in the NCFMASHO system. *Journal of Metamorphic Geology*, **24**, 783-802.
- Weber, S. & Bucher, K., 2015. An eclogite-bearing continental tectonic slice in the Zermatt-Saas high-pressure ophiolites at Trockener Steg (Zermatt, Swiss Western Alps). *Lithos*, **232**, 336-359.
- Weber, S., Sandmann, S., Miladinova, I. *et al.*, 2015. Dating the initiation of Piemonte-Liguria Ocean subduction: Lu-Hf garnet chronometry of eclogites from the Theodul Glacier Unit (Zermatt-Saas zone, Switzerland). *Swiss Journal of Geosciences*, **108**, 183-199.
- Whitney, D. L. & Evans, B. W., 2010. Abbreviations for names of rock-forming minerals. *American Mineralogist*, **95**, 185.
- Yardley, B. W., 2009. The role of water in the evolution of the continental crust. *Journal of the Geological Society*, **166**, 585-600.
- Zack, T. & John, T., 2007. An evaluation of reactive fluid flow and trace element mobility in subducting slabs. *Chemical Geology*, **239**, 199-216.
- Zheng, Y.-F., 1993. Calculation of oxygen isotope fractionation in anhydrous silicate minerals.

*Geochimica et Cosmochimica Acta*, **57**, 1079-1091.

Zheng, Y.-F., 1999. Oxygen isotope fractionation in carbonate and sulfate minerals.

*Geochemical Journal*, **33**, 109-126.

## SUPPORTING INFORMATION

**Figure S1:** Additional field and petrological figures. **(a)**. Field picture of a mafic boudin wrapped in a quartz-eclogite showing a nearly continuous rim of garnetite around the boudin. **(b)**. Field view of a brecciated, metasomatized eclogite in the ASZ showing mylonitized clasts cemented by omphacite and pseudomorphs after lawsonite. The structures shown recall the eclogite breccia described by Angiboust *et al.* (2012) in the Monviso ophiolitic massif further south. **(c)**. Eclogitized granulite (with remnants of pre-Alpine garnet) crosscut by a domain comprising omphacite and numerous cm-sized, lozenge-shaped aggregates interpreted as pseudomorphs after lawsonite (now filled by clinozoisite + paragonite). **(d)**. Field picture from the rim of a mafic block (ASZ) showing the formation of clinozoisite associated with very pervasive mylonitization (and alternation of omphacite and clinozoisite layers). **(e)**. BSE image of a garnet crystal from a mafic eclogitic mylonite from the ASZ (see Fig. 8c) showing replacement of garnet by clinozoisite, and wrapping within an eclogite-facies foliation. **(f)**. Close up view on mineral inclusions in garnet from picture (e). Rare and small phengite inclusions are visible associated with clinozoisite, omphacite and diopside in garnet cores (orange circles).

**Table S1:** GPS coordinates for the samples.

**Table S2:** THERMOCALC average *P-T* results for non-metasomatized and metasomatized eclogites from the Mt. Emilius klippe.

**Table S3:** Carbon and O isotope compositions of calcite veins and marbles/calc-silicates from the ASZ.

Received 27 May 2016; revision accepted 4 December 2016.

## FIGURE and TABLE CAPTIONS

**Figure 1: (a):** Geological map of the studied region in NW Italy (see inset) modified and simplified after Steck *et al.* (1990). The Zermatt-Saas Unit (ZSU) is overlain by a series of

tectonic slices of continental affinity: the Etirol-Levaz unit (ELU), the Theodul Glacier Unit (TGU), the Glacier-Raffray unit (GRU), the Chatillon unit (ChU) and the Mt. Emilius unit (EMU). These slices, that all contain remnants of Permian granulite-facies metamorphism, have been eclogitized during Alpine subduction. Localities studied in the EMU massif containing *HP* vein systems (yellow stars) are the following: Bon Plan (BP), Saint Marcel (SM), Grauson (GR), Laures (LA) and Arbole (AR). **(b)**. Detailed geological map (modified after Pennacchioni, 1996) of the Arbole sector (red square in a) showing the imbrication of metabasitic layers within the host paragneiss. **(c)**. *P-T* estimates for the ELU, TGU and ZSU (see references in text; background grid from Angiboust *et al.*, 2009). Peak estimates for EMU are from this work.

**Figure 2:** **(a)**. Simplified sketch showing field structural relationships within the Arbole shear zone between metasomatized fragments and host garnet micaschists. **(b)**. Field view of a dismembered garnetite layer wrapped by a Czo-rich, eclogite-facies foliation.

**Figure 3:** Sample and field pictures showing textural relationships between vein systems and host rocks in the ASZ sector. **(a)**. Folded and fractured garnetite layers and a vein filled by fibrous clinopyroxene. **(b)**. Host granulite (only partly re-equilibrated during the Alpine stage) cut by a coarse-grained vein filled by fibrous clinopyroxene, blocky quartz (and pyrite). **(c)**. Field view of a garnetite layer cut by a network of calcite-rich veins. **(d)**. Picture of a specimen showing euhedral grossular and clinopyroxene crystals filling a calcite vein. **(e)**. Foliated and fractured eclogite showing a garnet vein obliquely transected by a clinopyroxene vein. **(f)**. Typical fractured garnetite (comprising rounded, greenish pseudomorphs after pre-alpine diopside  $Di_0$ ; white arrow) first cut by a vein containing fibrous clinopyroxene and later cut by a clinozoisite vein.

**Figure 4:** Field and sample pictures showing the representative texture of vein systems in the Arbole region (a, b and c), in the Grauson sector (d) and in Saint Marcel valley (see Fig. 1a for location). **(a)**. Fine-grained garnet-clinopyroxene-clinozoisite metasomatized matrix cut by clinopyroxene veins that may have formed via hydrofracturing (ASZ). **(b)**. Clinopyroxene-rich host cut by a clinozoisite-rich hydrofracture containing angular clasts from the host (ASZ). The clinozoisite-rich domain may have been formed by pure lawsonite under peak metamorphic conditions within the lawsonite stability field (see discussion). **(c)**. Garnetite clast floating within calcite (ASZ). **(d)**. Outcrop view of a quartz-bearing hydrofracture system transecting perpendicularly the felsic gneiss matrix. Locally, cm-sized rutile needles can be found embedded within these quartz veins (inset). **(e)**. Omphacite-bearing quartz vein cutting through a felsic gneiss (Saint Marcel valley).

**Figure 5:** Scanning Electron Microscope images (back-scattered imaging mode) showing micro-textures visible in ASZ garnetites. **(a)**. Rounded pseudomorphs after a pre-alpine diopside (now replaced by another generation of clinopyroxene) surrounded by garnet. **(b)**. Garnetite clast exhibiting an internal foliation (clinozoisite bands, aligned clinopyroxene inclusions) abruptly cut by a clinopyroxene and clinozoisite vein. Omphacite is present both as inclusion within the clast as well as within the vein, associated with diopside. **(c)**. Internal texture of a garnetite showing an intra-garnet “pseudo-foliation” comprising numerous, aligned titanite grains. Clinopyroxene and clinozoisite precipitate along with garnet. The white arrow points to garnet-clinopyroxene grain boundary suggesting coeval formation. **(d)**. Close up view of the garnetite matrix showing the xenomorphic appearance of garnet and the very complex imbrication of garnet grains (see inset). **(e)**. Image showing a pre-alpine diopside  $Di_0$  pseudomorph included within a garnetite. Multiple replacement stages of the pre-alpine darker diopside  $Di_0$  are visible. This crystal is now cross-cut by two generations of chemically distinct clinopyroxene. **(f)**. Replacement of a pre-alpine diopside  $Di_0$  crystal from a garnetite showing re-equilibration by a Na/Fe-richer clinopyroxene composition along the former cleavages (and along microcracks).

**Figure 6:** **(a)**. Representative BSE image showing the equilibrium texture within calcite-bearing veins between oscillatory garnet (black arrow), calcite, clinozoisite and diopside. **(b)**. BSE image showing a former titanite porphyroclast micro-fractured and replaced by another titanite generation along its rims. Apatite is intergrown with the second titanite generation and surrounds Ttn1 crystals. Ttn2 contains almost 1% more  $Al_2O_3$  than Ttn1. **(c)**. X-ray maps from a garnet crystal showing oscillatory pattern from a calcite vein (Fig. 3d). **(d)**. BSE image showing a first clinopyroxene vein generation (containing garnet) cut and overgrown by a newer fibrous clinopyroxene vein. **(e)**. BSE image revealing the internal structure of a clinopyroxene vein showing three stages. A first diopside (light grey) is fractured and overgrown by an omphacite-rich Cpx (dark grey). This symmetric structure is lately fractured and healed by another Cpx generation (medium grey). **(f)**. Optical microscope image showing a garnet vein cross-cutting obliquely the Cpx-rich matrix. Numerous, stretched inclusions of clinopyroxene are trapped within garnet.

**Figure 7:** **(a)**. BSE image of a large poly-metamorphic garnet from an eclogitized granulitic boudin in the vicinity of the Arbole shear zone. This crystal exhibits an atoll-like texture showing darker relicts of fractured pre-Alpine garnet ( $Grt_0$ ), rimmed and replaced along the cracks by a brighter Alpine  $Grt_1$  generation. The pre-Alpine garnet has been dissolved and replaced by clinopyroxene, chlorite and quartz. Replacement has not proceeded along the

bright Alpine cracks. **(b)**. Sketch simplifying the microstructure described in (a). **(c)**. X-ray map from a garnet from an eclogitized granulitic boudin outside the ASZ preserving relics of a pre-alpine  $Grt_0$  now rimmed, dissolved and replaced by an Alpine  $Grt_1$  generation along its cracks. Note the absence of Ca enrichment along the cracks (with low XMg), suggesting post-healing Ca enrichment.

**Figure 8:** **(a)**. Combined BSE image and X-ray map (Mn, counts) of a fractured garnet porphyroclast from a metasomatized mafic eclogite from the Arbole shear zone. This image shows that  $Grt_1$  possesses a normal “Alpine” prograde zoning (with decreasing Mn concentration). The new garnet 2 generation that overgrows  $Grt_1$  is Ca- and Mg-richer, poorer in Fe, and forms within the tensile crack in equilibrium with diopside. **(b)**. X-ray map of the same garnet crystal (Fe, counts) showing dissolution of  $Grt_1$  and replacement by  $Grt_2$  and clinozoisite (white arrow). **(c)**. Comparison of ASZ garnet compositions showing very high grossular contents, especially for garnet analyses from garnetite pods. The scanned thin section to the right of the triangle localizes the various microdomains encountered within a single specimen. **(d)**. BSE image of a garnet aggregate from the Czo+Di domain (see c) showing various stages of dissolution (see inset) and precipitation of a darker, Ca-richer garnet composition. One omphacite inclusion has been observed within a  $Grt_1$  crystal remnant. Omphacite is absent from the matrix around the garnet here. **(e)**. X-ray map (Mn, Ca and Fe) of a part of the garnetite pod showing the extreme complexity of the zoning pattern with multiple dissolution, fracturing (white arrow) and replacement stages. Oxide weight contents measured at the electron probe are given for reference.

**Figure 9:** Composition of clinopyroxene crystals from mafic eclogites and garnetites from the ASZ as a function of their microtextural position (see Figs 5 & 6). Clinopyroxene composition is plotted in the Jd-Hed-Di system since the Ca-Tschermak molecule is absent (or very low) in ASZ samples. This figure highlights the presence of Na-rich minerals in all textural positions as well as the prevalence of Na-poor compositions along the Alpine foliation.

**Figure 10:** Comparison of whole-rock compositions in the Ca-Na-Mg system. Data from mafic rocks from the Ivrea zones from Sills & Tarney (1984) and Mazzucchelli *et al.* (1992). This figure shows that potential protolith analogues are slightly poorer in CaO and richer in Na<sub>2</sub>O and MgO. Rock compositions from this work have been estimated using both Scanning Electron Microscopy technique (SEM-EDS) and X-ray fluorescence chemistry (XRF).

**Figure 11:** Al-Ca-F(Fe-Mg-Mn) projection showing phase relationships between various peak

metamorphic minerals from the ASZ and from potential pre-metasomatic analogues. The grey-shaded domain reflects the projected area for the range of protolith compositions. Ivrea mafic bodies composition is from Sills & Tarney (1984).

**Figure 12:** Comparison of  $\delta^{13}\text{C}$  and  $\delta^{18}\text{O}$  of calcite veins and marble/calc-silicates from the ASZ (see data in Table S3) with values for calcite in other *HP* lithologies in the Penninic domain, including the Zermatt-Saas unit (ZSU) and the Monviso massif (MV; data from Cook-Kollars *et al.*, 2014; Collins *et al.*, 2015). The grey arrow indicates the trajectory in O and C isotope compositions followed by a rock undergoing decarbonation by a Rayleigh process.

**Figure 13:** Conceptual view (not to scale) showing one possible model explaining the structures and processes observed in the Arbole Shear Zone (black square). In our model the thrust surface at the bottom of the Mt. Emilius slice represents a former subduction interface after peak metamorphic accretion. The closest analogue to the downgoing plate exposed now in the field is represented by the Zermatt-Saas unit (Fig. 1). This figure proposes the infiltration of slab-derived fluids, leading to the progressive transformation of pre-Alpine granulites into garnet micaschists during Alpine metamorphism at *HP* conditions. Some of the hydrofractures observed in the field (Figs 3b & 4) and crosscutting the base of the massif are considered as potential fluid pathways that enabled the transport of external fluids towards the core of the Mt. Emilius slice. The Arbole shear zone corresponds to a former mafic layer (possibly a mafic intrusion) around which deformation localized (Fig. 2). Garnetites (such as the ones shown in Fig. S1a) from the metasomatized domain are depicted as red pods and marble lenses as blue layers. Note that peak metamorphic structures (such as the ASZ and the veins systems) depicted on this sketch have been subject to transposition and parallelization to the basalt thrust during an exhumation-related, greenschist-facies deformation event.

**Table 1:** Summary of cross-cutting relationships and structural evolution of the various vein generations observed in the Mt. Emilius massif and in the Arbole Shear Zone.

**Table 2:** Representative mineral analyses from the ASZ metasomatized eclogites.

**Table 3:** Bulk-rock compositions determined by X-ray fluorescence. (\*): data from Sills & Tarney (1984) and (\*\*) from Mazzucchelli *et al.* (1992) for mafic boudins from the Ivrea zone which constitute potentially good analogues for the pre-metasomatic protolith of ASZ rock samples. Sample #15-02 corresponds to a non-metasomatized lithology.

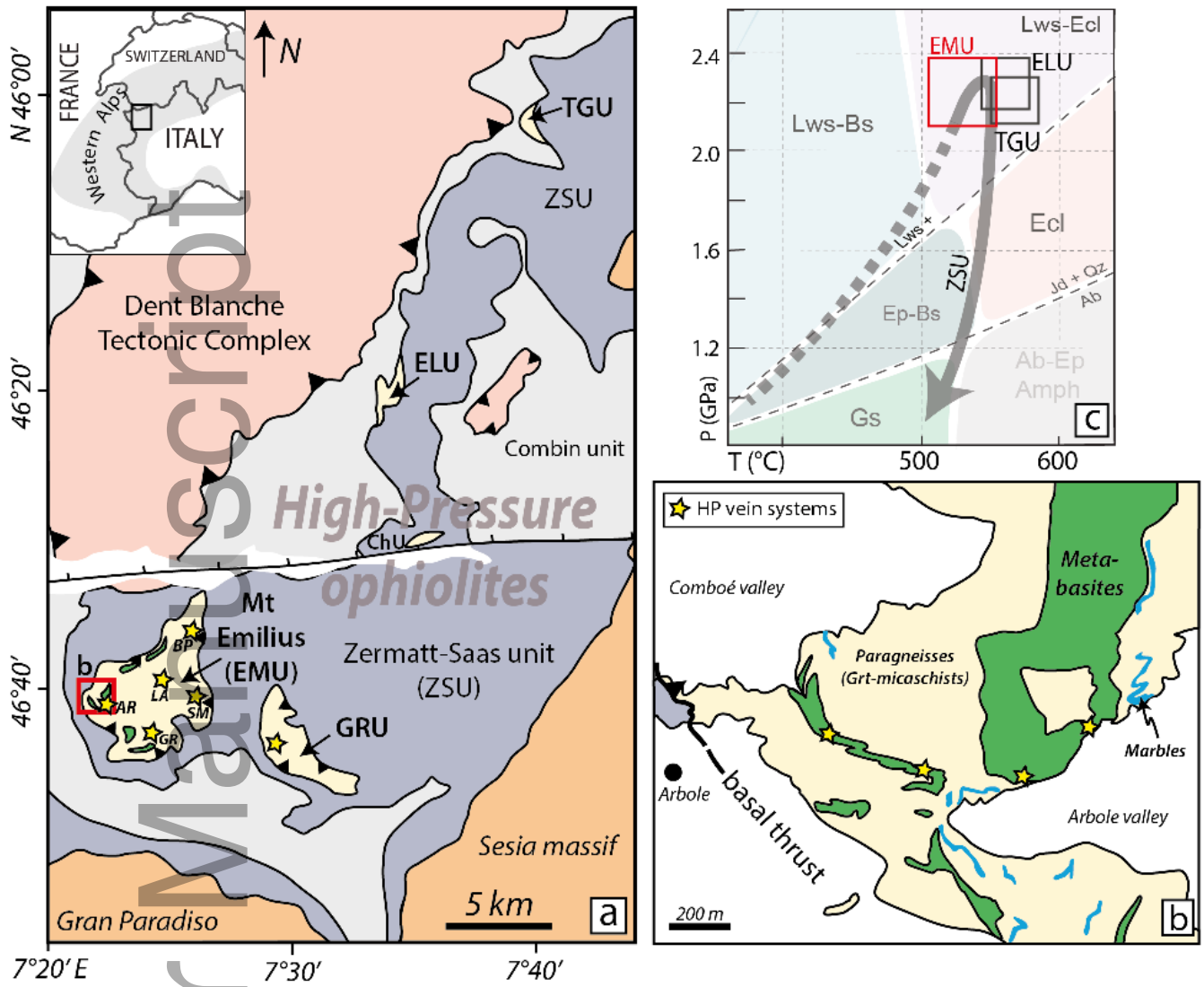


Figure 1

jmg\_12241\_f1.tif

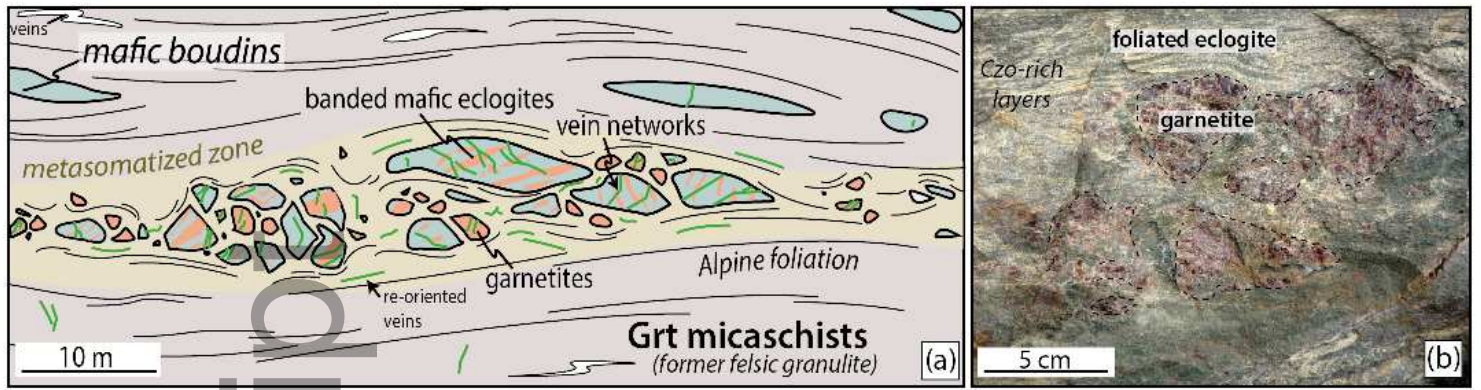


Figure 2

jmg\_12241\_f2.tif

Author Manuscript

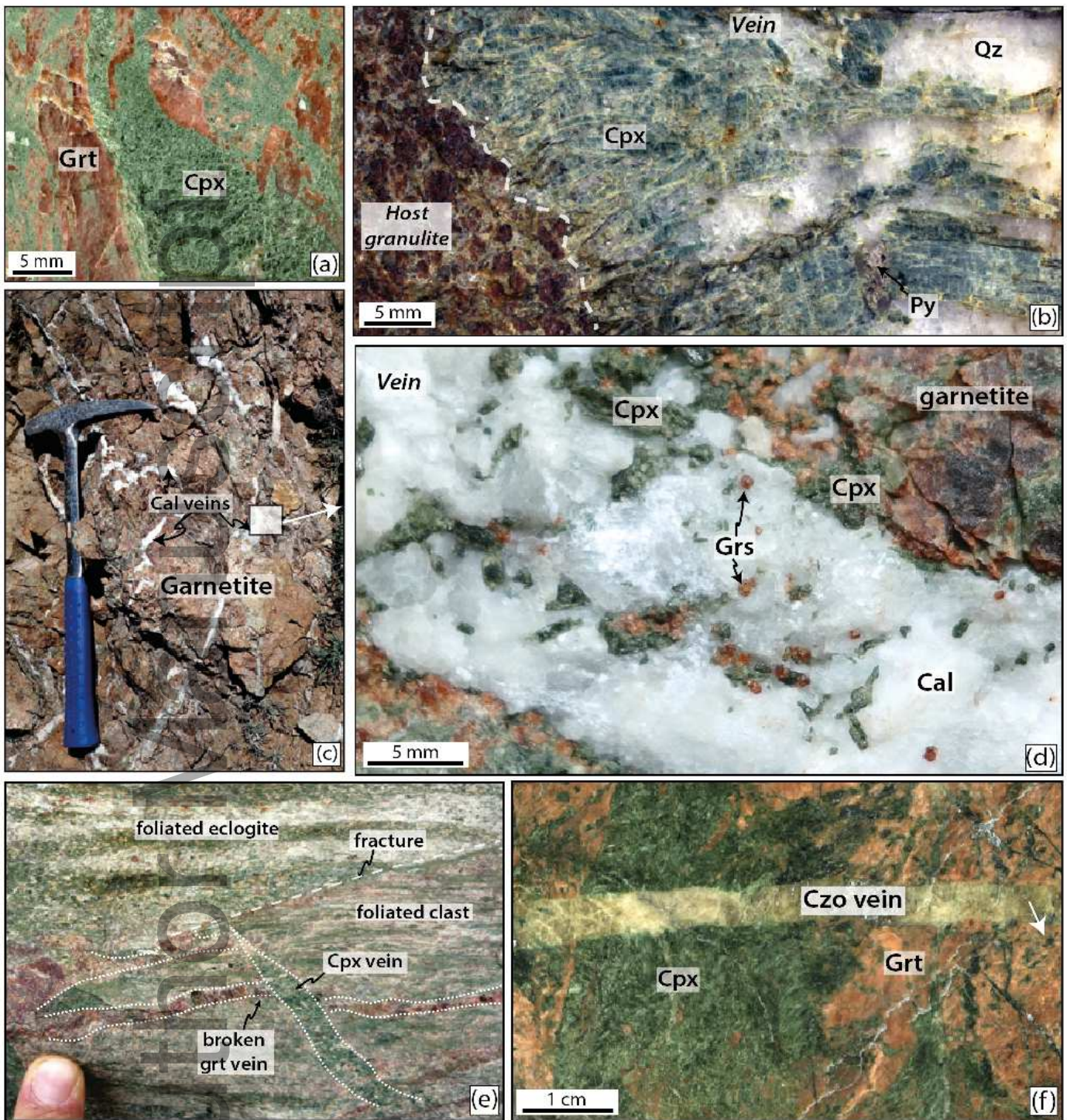


Figure 3

jmg\_12241\_f3.tif

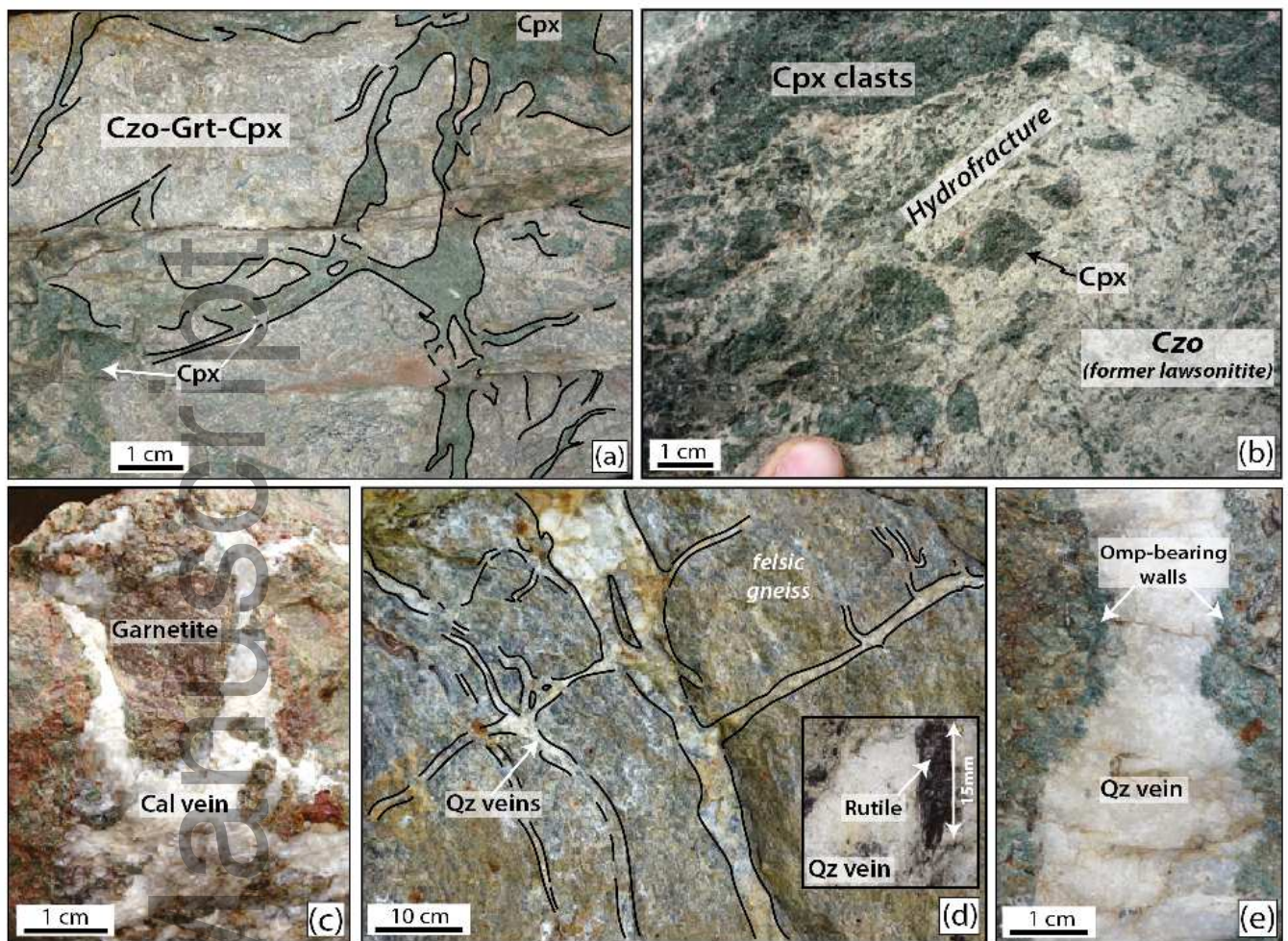


Figure 4

jmg\_12241\_f4.tif

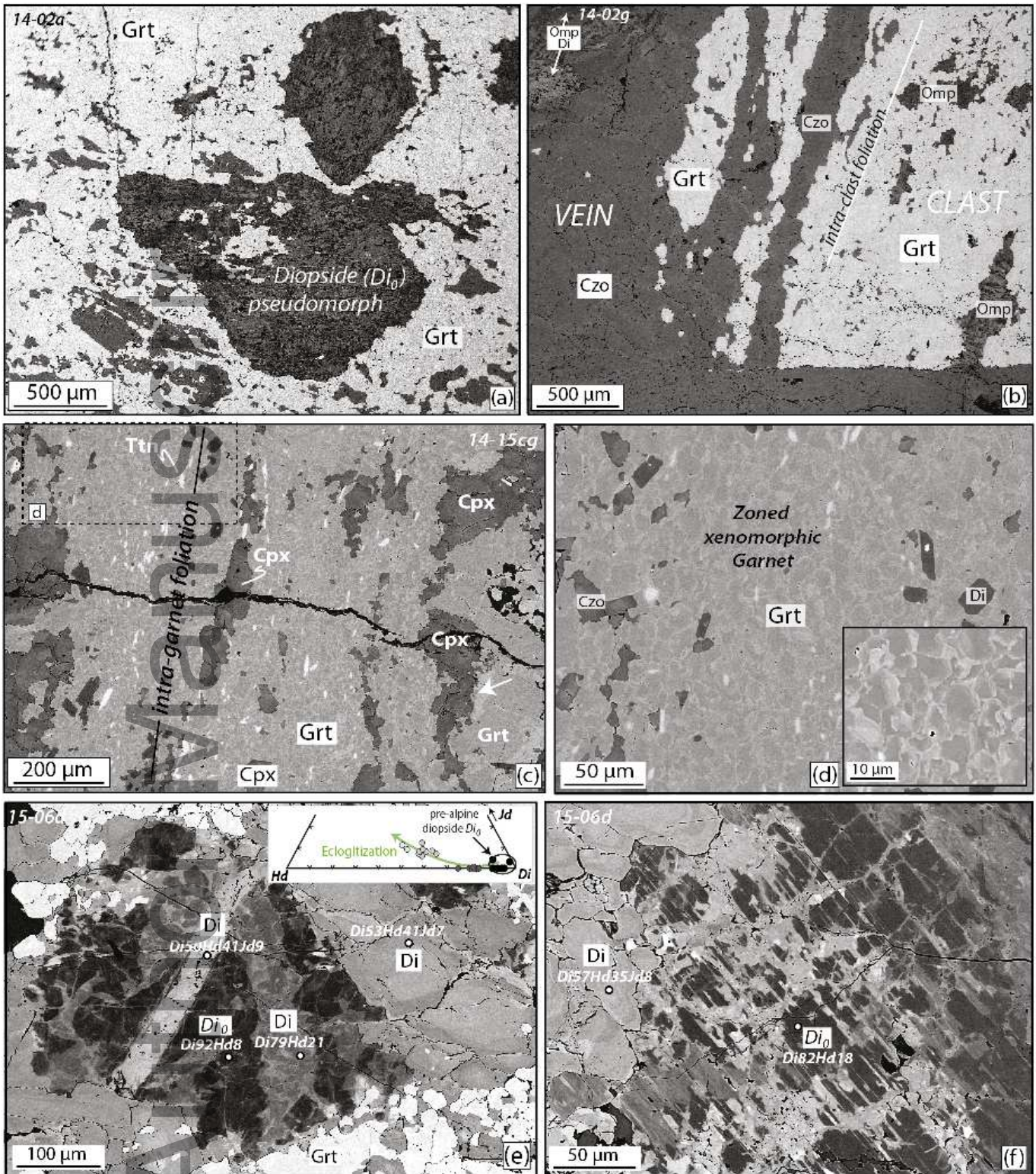


Figure 5

jmg\_12241\_f5.tif

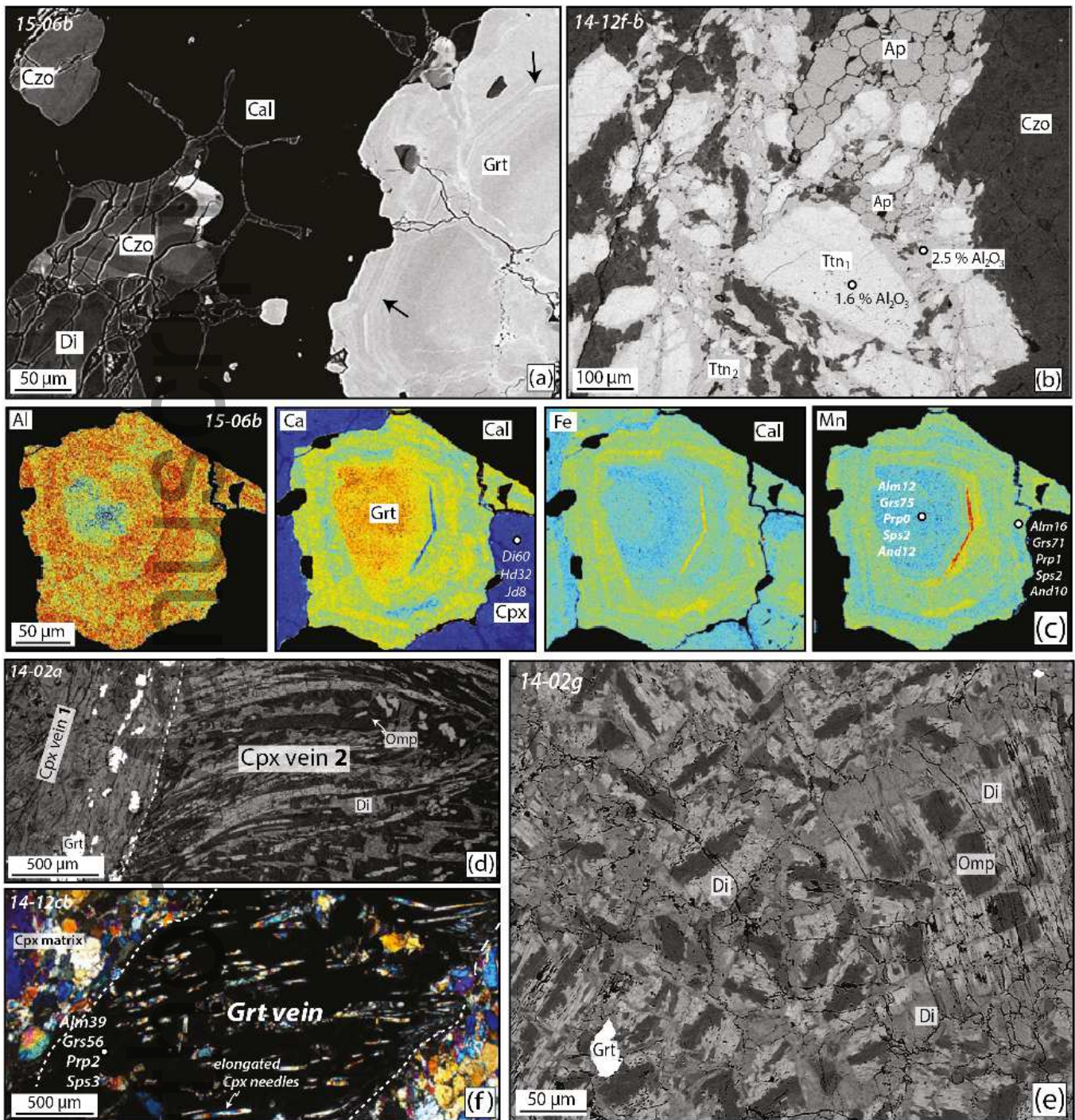


Figure 6

jmg\_12241\_f6.tif

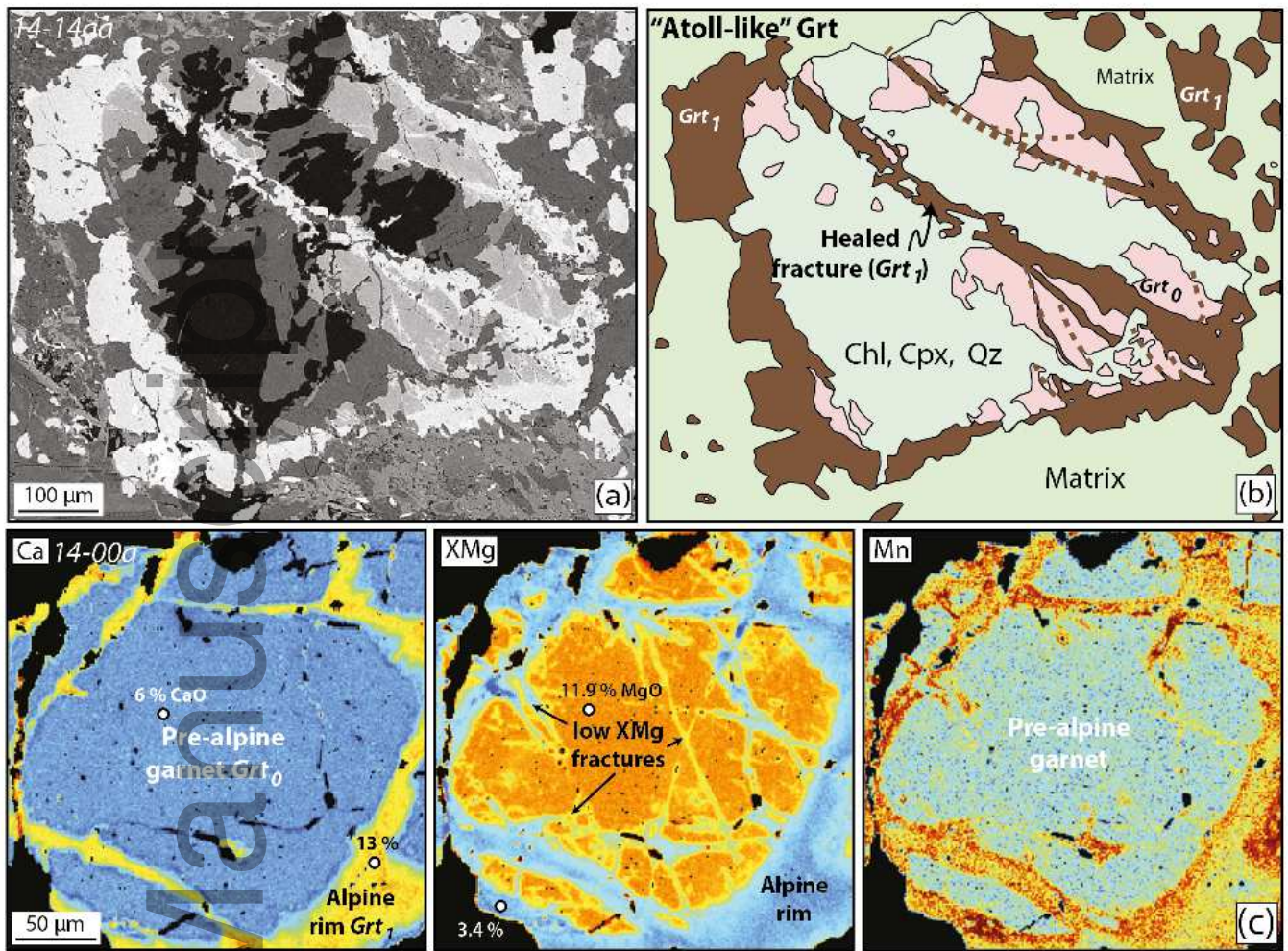


Figure 7

jmg\_12241\_f7.tif

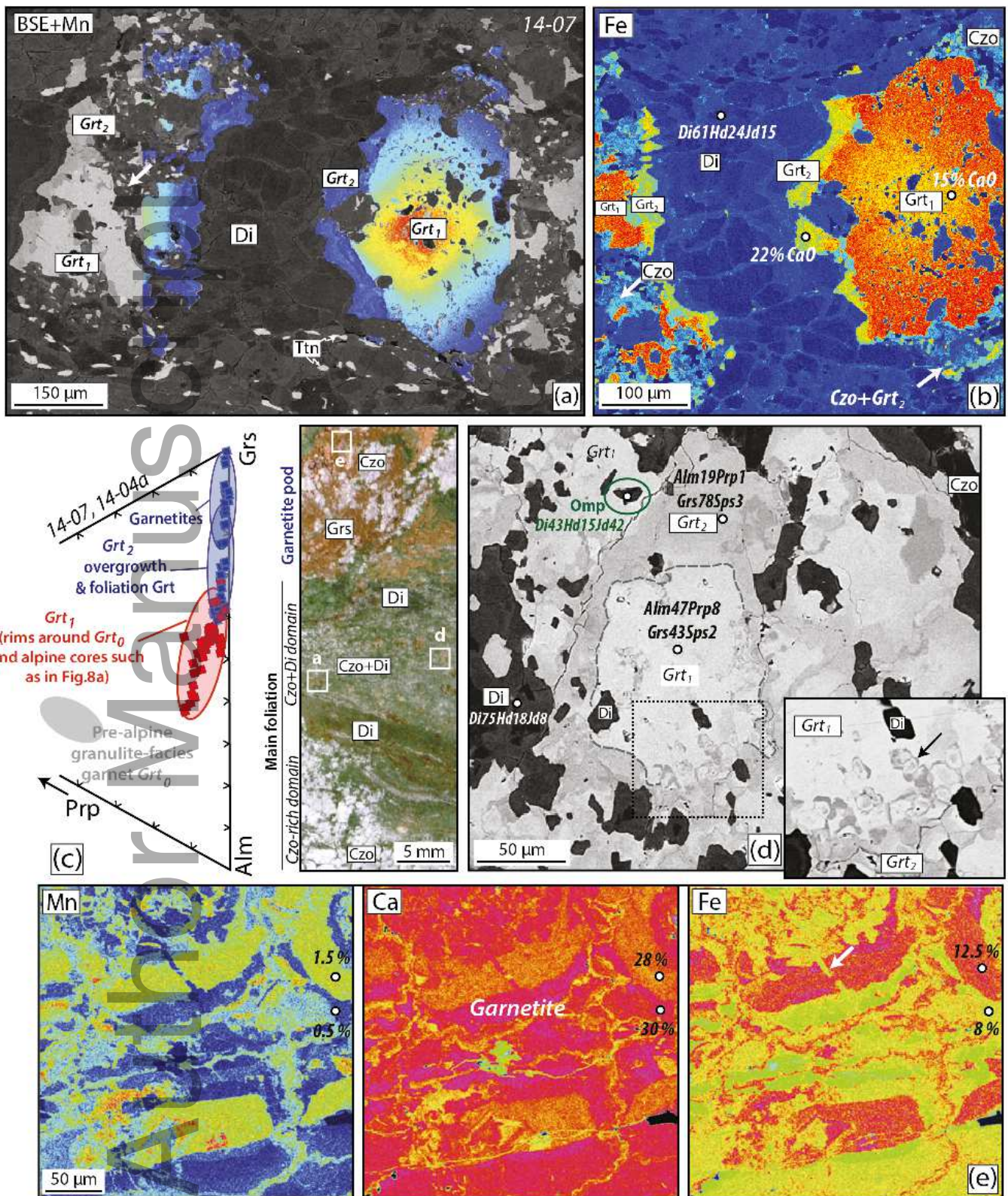


Figure 8

jmg\_12241\_f8.tif

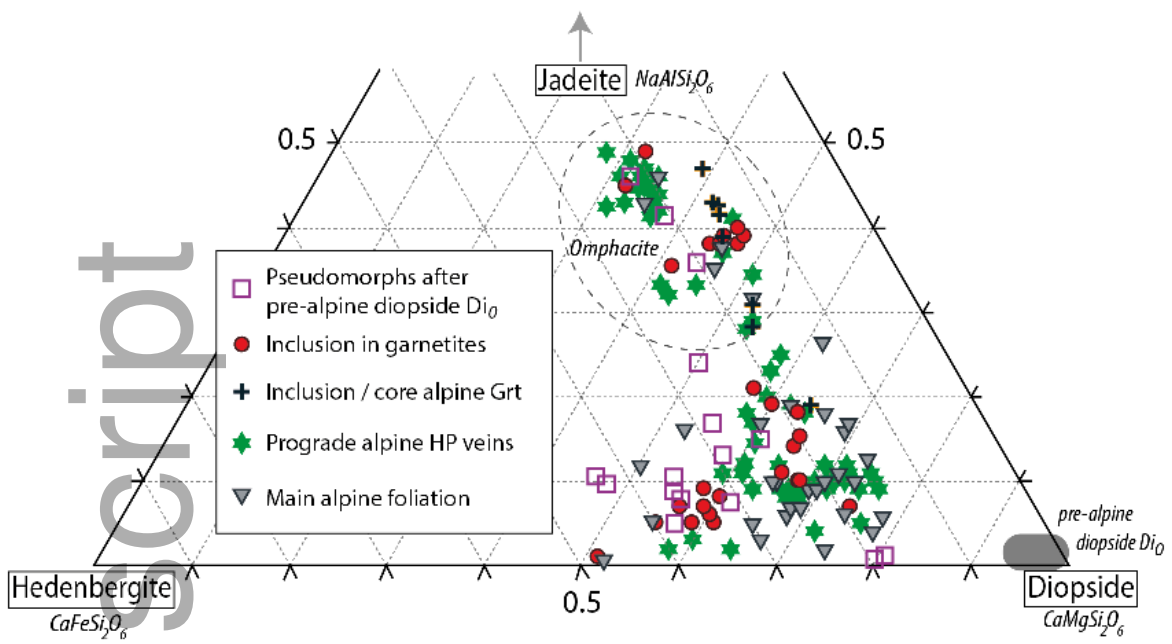


Figure 9

jmg\_12241\_f9.tif

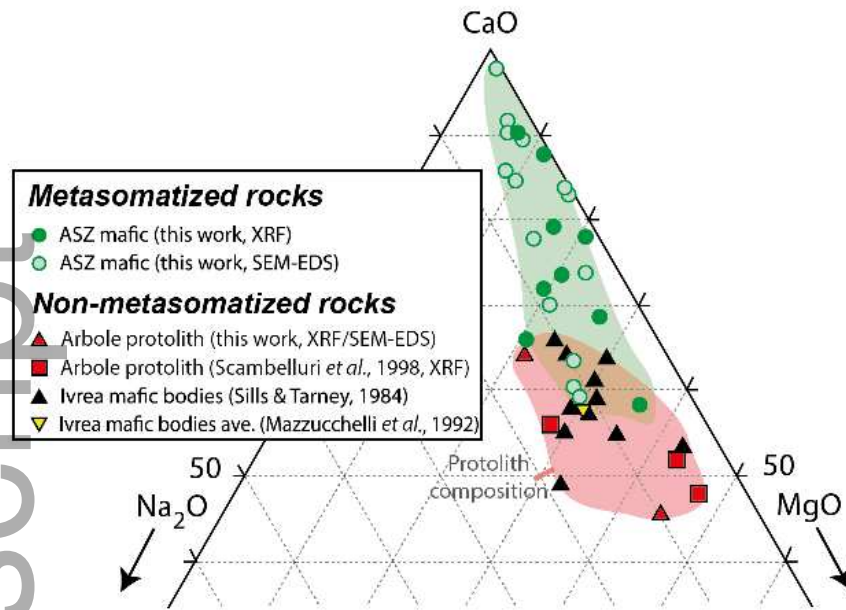


Figure 10

jmg\_12241\_f10.tif

Bulk-rock compositions		Mineral analyses	
+ Metasomatized ASZ rocks (+ garnetites)		• Garnet	+Ttn
+ Non-metasomatized ASZ rocks		□ Epidote/Czo	+H <sub>2</sub> O
+ Ivrea mafic bodies		▲ Omphacite/Cpx	+Ap
			+Qz
			+MgFe-1
			+KNa-1
			+SiNaAlCa-1
			+MnFe-1

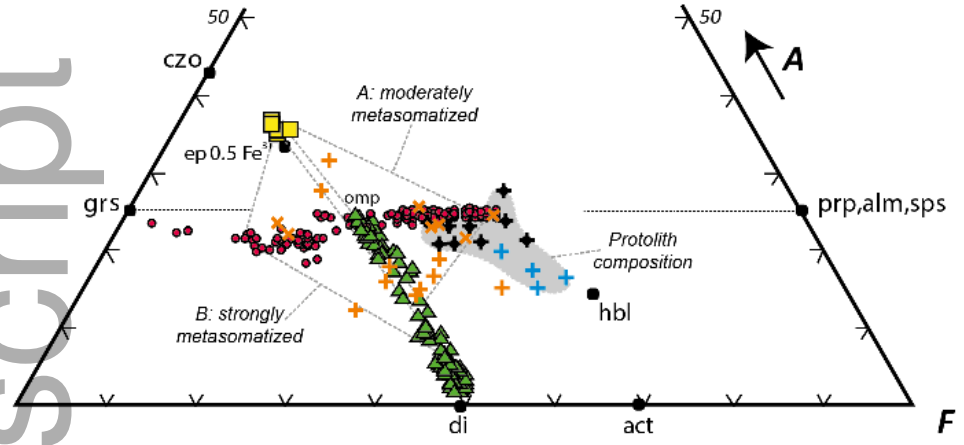


Figure 11

jmg\_12241\_f11.tif

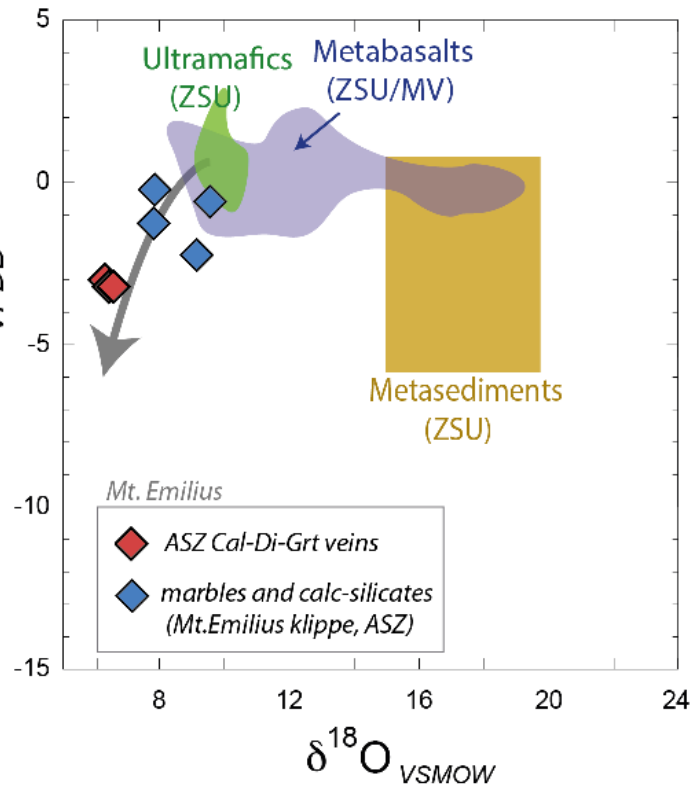


Figure 12

jmg\_12241\_f12.tif

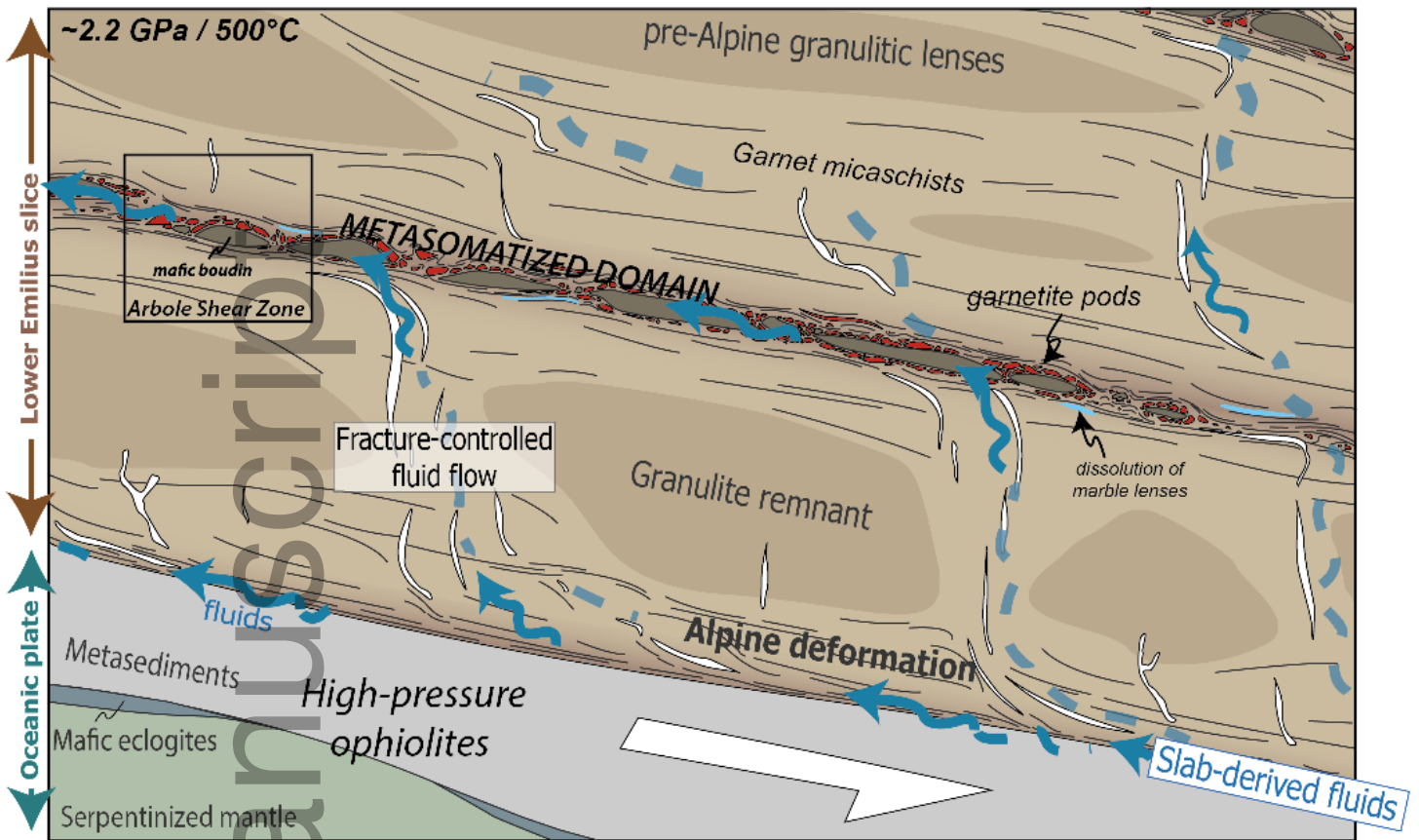


Figure 13

jmg\_12241\_f13.tif